Improving Transient Stability of an Islanded Microgrid Using PV Based Virtual Synchronous Machines

W.P.M. NISITHA U. PADMAWANSA

178522F

Thesis submitted in partial fulfilment of the requirement for the degree of Master of Science

Department of Electrical Engineering

University of Moratuwa

Sri Lanka

January 2020

Declaration of The Candidate and Supervisor

I declare that this is my own work and this thesis does not incorporate without acknowledgement any material previously submitted for a Degree or Diploma in any other University or institute of higher learning and to the best of my knowledge and person except where the acknowledgement is made in the text.

Also, I hereby grant to University of Moratuwa the non-exclusive right to reproduce and distribute my thesis, in whole or in part in print, electronic or other medium. I retain the right to use this content in whole or part in future works (such as articles or books).

---------- ----------

Nisitha Padmawansa Date

The above candidate has carried out research for the Masters thesis under my supervision.

---------- ----------

Signature of the supervisor Date

(Dr. Lidula N. Widanagama Arachchige)

Abstract

Renewable energy integrations are increasing rapidly in this decade. Lot of countries like Denmark, German and United Kingdom have already set their own targets for renewable energy instigation in their future grids. When considering renewable energy power generation (Solar and wind), most of the time, inverters are used for grid integration. Conventional power generation is based on synchronous generators (Coal, Nuclear, Hydro). Due to the large integration of renewable power plants, power system is moving to a synchronous generator dominant power system to inverter dominant power system. This makes a significant impact on the system inertia response. Inertia is given from the rotating mass of the conventional generators but in inverters, as there are no any rotating masses, inverters cannot contribute to system inertia. Lack of inertia makes poor inertia response. When there is lack of inertia, system's ability to maintain stability under disturbances will be weakened, which would limit the integration of renewable sources. Microgrids, particularly PV-Hydro based Microgrids would be seriously affected from this issue.

This research is carried out to provide a solution for the aforementioned issue by emulating inertia through inverters. Since there are no any actual rotating parts, when emulating inertia through inverters, dynamic inertia response can be implemented compared to the static inertia in synchronous generators.

Due to disturbances in the system, the operation of solar PVs will also be affected. Because of that an energy management system is introduced to support virtual synchronous generator and to keep the PV plant operation at its maximum power point without interruption. The proposed controllers are verified through simulated PV-Hydro microgrid. Simulations are carried out using PSCAD.

Acknowledgements

Foremost, I would like to express my sincerer gratitude to my advisor Dr. Lidula N. Widanagama Arachchige for the continuous support for my MSc research. I am extremely thankful to her for providing such a nice support and guidance, although she had busy schedule.

I am grateful to all the lecturers of Electrical Engineering Department at University of Moratuwa for the guidance provided by them to success of this research, through their valuable comments.

I would also like to acknowledge Dr. Dharshana Muthumuni for give the opportunity to use PSCAD freely.

I would like to thankful for my colleagues and friends who have help and encourage throughout this research.

Finally, I must express my very profound gratitude to my family: my parents, brother and Dilini whose love and guidance are with me in whatever I pursue.

Table of contents

List of Figures

Abbreviations

ROCOF	Rate of change of frequency
VSM	Virtual synchronous machines
PV	Photovoltaic
MPPT	Maximum power point tracking
IGBT	Insulated gate bipolar transistor
SOC	State of charge
PLL	Phase lock loop
EMS	Energy management system
VSC	Voltage source converter
PWM	Pulse width modulation

Chapter 1: **Introduction**

1.1 Background

The World is moving towards more renewable energy resources because of its eco-friendly behaviour. There are many agreements, which provide evidence to this, such as the Paris agreement in December 2015 [1]. According to these agreements many countries have agreed to increase renewable power generation to improve clean energy production. Countries like Denmark, Ireland and Germany are rapidly installing renewable power plants. They are operating with an annual penetration of more than 20% at the national level [2]. United Kingdom set the target of 15% of their power generation being renewable by 2020 [3]. Sri Lanka has also set a target of 100% renewable power generation by the year of 2050 [4].

Most of these renewable sources are found as distributed power sources. Therefore, the concept of Microgrids becomes more familiar. A microgrid is a group of local grids with a number of renewable energy sources, energy storage, and domestic loads, which can be identified as an independent system with the capability to operate in either grid-connected or isolated mode, thus reducing a huge burden on the utility grids [5][6]. Predicted percentage of world renewable power generation from various types of renewable power sources in 2050 is given in Figure 1 [7].

Frequency is an indicator of balance between generation and demand of active power. In a synchronous generation-based system, primary frequency control is used to control the frequency by adjusting the prime movers with a droop control mechanism. Then the generation will be settling at its new steady state, which is equal to the system active power demand. Inertia response is the rate of change of frequency (ROCOF) as it approaches to its new steady state. Traditionally, this rate of change of frequency is determined by the stored kinetic energy in the rotating mass of the generators and the turbines in the system. Inherent inertia response of traditional generators will limit the frequency rate of change. It allows keeping the frequency within limits until the prime mover action is involved in traditional generators.

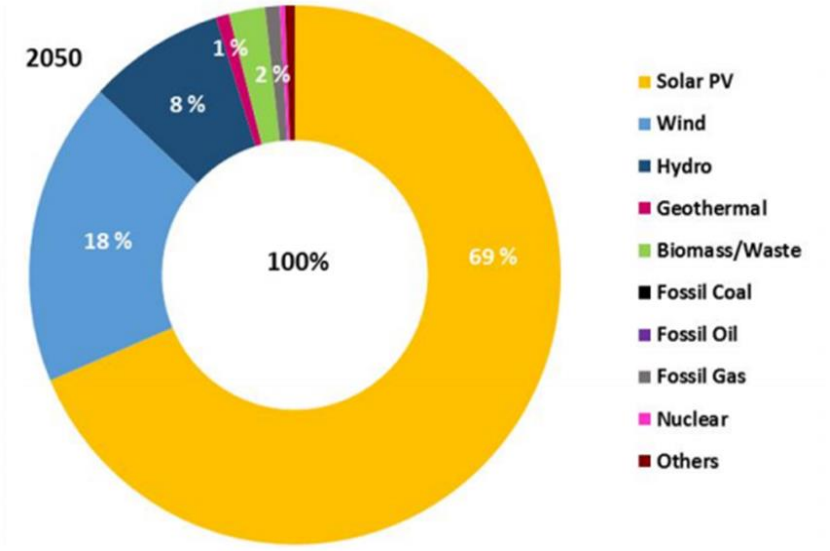

Figure 1: Electricity generation from renewables in 2050

Most of the dominant renewable power sources (solar and wind) deliver power via inverters. Therefore, inverter-based power sources are going to be a dominant part in future grids [8]. At present, inverter dominant power generation takes up a considerable part of the total power generation [9]. Because of the large penetration of renewable sources, inverter dominant power generation rose rapidly. Even though inverters help to connect more renewable sources to the system, since it does not supply any mechanical inertial response, it compromises the frequency stability of the system. Installing more inverter dominant power plants will further reduce the inertia response of the whole system, which will make the system more vulnerable for frequency fluctuations. Because of this effect integrating renewables to the system via inverters is limited by the system operators.

1.2 Problem Statement

Integrating more inverter dominant renewable sources like Solar PVs to Microgrids reduces the system's rotating inertia. This will reduce the total inertia response of the system. Due to this reason, the system frequency stability gets reduced. Finally, this will limit the integration of inverter dominant renewables to the system.

1.3 Motivation

Demand for the clean energy is increasing rapidly due to many reasons such as environment pollution, fuel prices laws and regulations etc. Most of the renewable power sources are connected to the system through inverters. Due to the lack of mechanical inertia in inverter dominant power sources, system frequency stability is reduced. Therefore, integration of inverter dominant renewable power sources into the system is limited. This is a barrier to the integration of cleaner energy to the system.

1.4 Objectives

The following objectives are to be covered in this thesis

- To design a PV based Virtual Synchronous Machine (VSM) with a variable inertia constant controller to improve the transient frequency stability of an islanded PV-Hydro microgrid.
- To implement an energy management system to harvest maximum renewable power and reduce the required energy storage capacity.

1.5 Thesis Outline

Chapter 2, literature review contains the methods of frequency controlling used in traditional operations and the help of inertia response in system frequency. This chapter contains a comparison of past used methods in virtual inertia emulating. Chapter 3, System Design, include the basic design of the Hydro-PV microgrid system. This chapter contains the description about the elements used in this microgrid system. Chapter 4 describes the two proposing controllers. Simulation model with the controllers is described in chapter 5. Simulation results are present in chapter 6 and discussion of the work is in chapter 7. At last, chapter 8 concludes the remarks and makes recommendations for further work.

Chapter 2: **Literature Review**

2.1 Frequency Control in Power Systems

For a satisfactory operation, the power system frequency must be nearly constant. This makes sure that the balance between power consumption and generation is kept. When the active power generation and consumption is balanced, the frequency will remain at system rated frequency. When there is mismatch between active power generation and consumption, there is sequence of controlling strategies involved in regaining the frequency to the system rated value. Figure 2 [9] shows the sequence of events that happen when there is a frequency deviation.

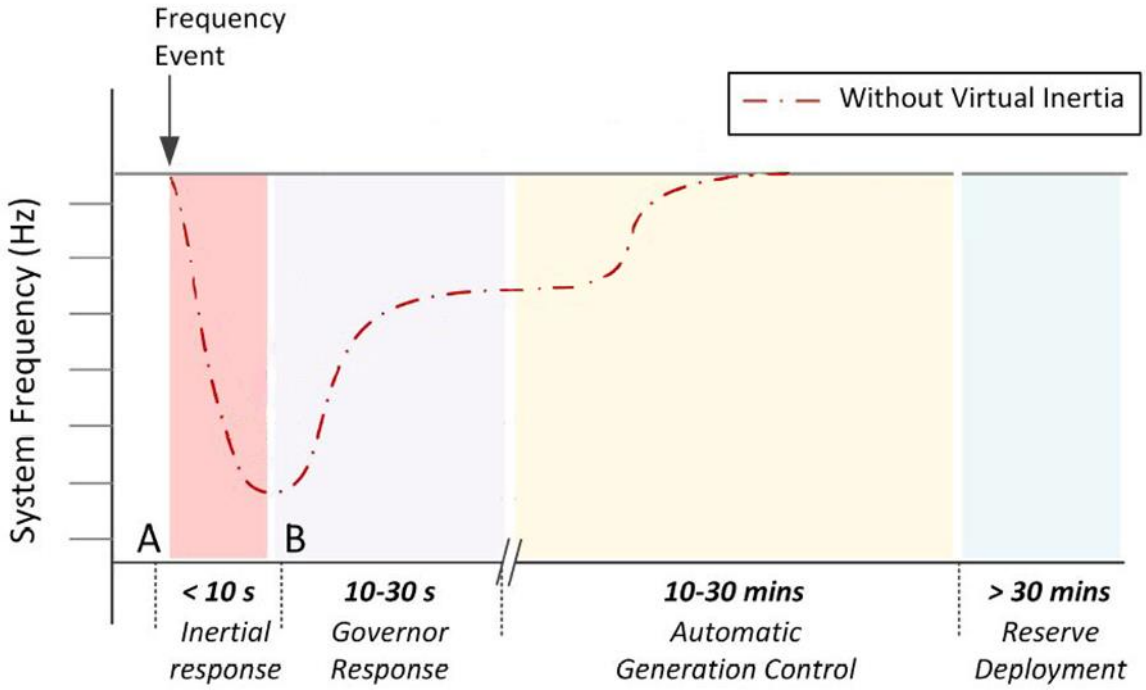

Figure 2:Sequence of events happen after a frequency deviation

2.1.1 Inertia Response

When an active power mismatch occurs between power generation and consumption, inertia response instantaneously takes place due to the stored system inertia in synchronous units. This will reduce the frequency deviation for a few seconds.

2.1.2 Primary Response

Afterwards, primary frequency response is involved. The primary frequency response is the turbine governor action or governor like action. This will increase or decrease the input power to the prime mover. Depending on the input power variation to the governor, the generator increases or decreases the active power generation proportional to system frequency deviation, which is followed by the inertia response.

2.1.3 Secondary Response

After the primary response, secondary response initiates. This employs the regulating reserves to take back frequency to its nominal value. This will make use of central

regulator, changing the active power set points of generators to exchange power within generator's boundary control areas to their programmed values to recover the frequency to the system set point. To provide an effective secondary control, generators, which are involved with secondary control, must have sufficient power reserved with both the required change in generated power and the required rate of change. Also, secondary response ensures that the full reserve to the primary response is available again. Secondary control takes part after about 30 s when the frequency deviation occurs and end within 15 minutes.

2.1.4 Tertiary Response

After the secondary response tertiary response takes part. This response refers to central coordination actions. It involves re-dispatching of the units and also possibly change unit commitment to restore the reserves which were utilized during the operation of previous responses in order to re-position the power system, so it can response to further events. Tertiary control is the last stage of the recovering process after a disturbance occur [10].

Summary of the sequence of events and their contribution under event of frequency deviation is shown in Table 1.

Table 1 : Summery of frequency responses

Response	Potential issues	Contribution
Inertia response (Few seconds)	Low system inertia Low primary response time	Synchronous and asynchronous generators/motors
Primary response (10s-30s)	Lacking primary reserve Slow activation time of primary resource	Every running primary controlled generators in the system
Secondary response (30s-15minutes)	Lack of the secondary reserve delay of secondary resource	Load shared by Generators in the area of disturbance is regulated by load dispatch centre
Tertiary response	Lack of tertiary response Manual activation no frequency response	All generation contracted with the system.

2.2 Inertia Response

Inertia response is the 1st line of defence against the frequency fluctuations. This will help to keep the frequency within standard limits until the primary response involved. Inertia response is determined by the system inertia [9].

From Newton's second law,

$$J\frac{d\omega_m}{dt} + D_d\omega_m = \tau_t - \tau_e \quad (1)$$

Where *J* is the total (Generator and the Turbine) moment of inertia (kgm^2), ω_m is the rotor shaft velocity (mechanical rad/s), D_d is the damper torque coefficient (Nms), τ_t is the torque produced by the turbine (Nm) and τ_e is the counteracting electromagnetic torque (Nm).

Rotor position with respect to the synchronously rotating axis is define by the rotor or power angle, δ. Rotor velocity can be express as,

$$\omega_m = \omega_{sm} + \Delta\omega_m = \omega_{sm} + \frac{d\delta_m}{dt} \quad (2)$$

Where δ_m is rotor angle expressed in mechanical radians and $\Delta\omega_m = \frac{d\delta_m}{dt}$ is the speed deviation in mechanical radians per second. Therefore, from equations (1) an (2),

$$J\frac{d^2\delta_m}{dt^2} + D_d(\omega_{sm} + \frac{d\delta_m}{dt}) = \tau_t - \tau_e \quad (3)$$

Turbine torque, $\tau_t$changes slowly because of the high time constant of the rotor. But, τ_e can change suddenly. In steady state, rotor is rotating in synchronous speed (ω_{sm}). Turbine torque (τ_t) is equl to the sum of the electromagnetic torque, τ_e and the damping (rotational losses) torque, $D_d\omega_{sm}$ as given in (4),

$$\tau_t = \tau_e + D_d\omega_{sm} \quad (4)$$

Mechanical Torque τ_m can be define as equation (5),

$$\tau_m = \tau_t - D_d\omega_{sm} = \tau_e \quad (5)$$

From equations (2) and (4),

$$J\frac{d^2\delta_m}{dt^2} + D_d\frac{d\delta_m}{dt} = \tau_m - \tau_e \quad (6)$$

Multiply equation (6) by the synchronous speed ω_{sm} ,

$$J\omega_{sm}\frac{d^2\delta_m}{dt^2} + D_d\omega_{sm}\frac{d\delta_m}{dt} = \tau_m\omega_{sm} - \tau_e\omega_{sm} \quad (7)$$

$$J\omega_{sm}\frac{d^2\delta_m}{dt^2} + D_d\omega_{sm}\frac{d\delta_m}{dt} = P_m\frac{\omega_{sm}}{\omega_m} - P_e\frac{\omega_{sm}}{\omega_m} \quad (8)$$

Where P_m is the net shaft power input and P_e is the electrical air-gap power. During a disturbance, the speed of the synchronous machine is quite similar to the synchronous speed therefore, $\omega_{sm} \approx \omega_m$. Therefore, equation (8) becomes,

$$J\omega_{sm}\frac{d^2\delta_m}{dt^2} + D_d\omega_{sm}\frac{d\delta_m}{dt} = P_m - P_e \quad (9)$$

Equation (9) represents the connection with the moment of inertia and the active power mismatch between generation and demand. Comparing the inertia effect with the damping components (losses), damping component can be neglected. With that equation (9) can be further reduced as,

$$J\omega_{sm}\frac{d^2\delta_m}{dt^2} = P_m - P_e \quad (10)$$

Having a large synchronous generator means it has higher rational mass, which means having a higher moment of inertia constant. Higher moment of inertia constant will act as a large barrier for frequency deviations.

2.3 Inertia Constant

Inertia constant gives a clear idea about how much of the kinetic energy involved in the system compared with the total MVA capacity of the system.

$$Inertia\ Constant\ (H) = \frac{Kinetic\ Energy\ Store\ in\ Rotor\ (MW.s)}{MVA\ Rating} \quad (11)$$

Following equation can be obtain using combing equation 9 and 10

$$2H\frac{S_{rated}}{\omega_{sm}^2}\omega_{sm}\frac{d^2\delta_m}{dt^2} = P_m - P_e \quad (12)$$

The above equation can be simplified by dividing S_{base}

$$\frac{2H}{\omega_{sm}}\frac{d^2\delta_m}{dt^2} = P_{m\_pu} - P_{e\_pu} \quad (13)$$

Where P_{m_pu} and P_{e_pu} are the per unit components of P_m and P_e respectively. Equation (13) is also known as the swing equation. Typical inertia constant values are presented in the Table 2 [11].

Table 2: Typical Values for inertia constant

Type of Generating unit	H (s)
Thermal unit 3600 r/min (2-pole) 1800 r/min (4-pole)	 2.5 to 6.0 4.0 to 10.0
Hydraulic unit	2.0 to 4.0

2.4 Loss of Inertia in Future Power Systems

Most of the countries are now trying to integrate more renewable energy for their power system. Electrical energy demand is rapidly increasing and at the same time need for reduced environmental pollution is growing. As a result, world's power generation is

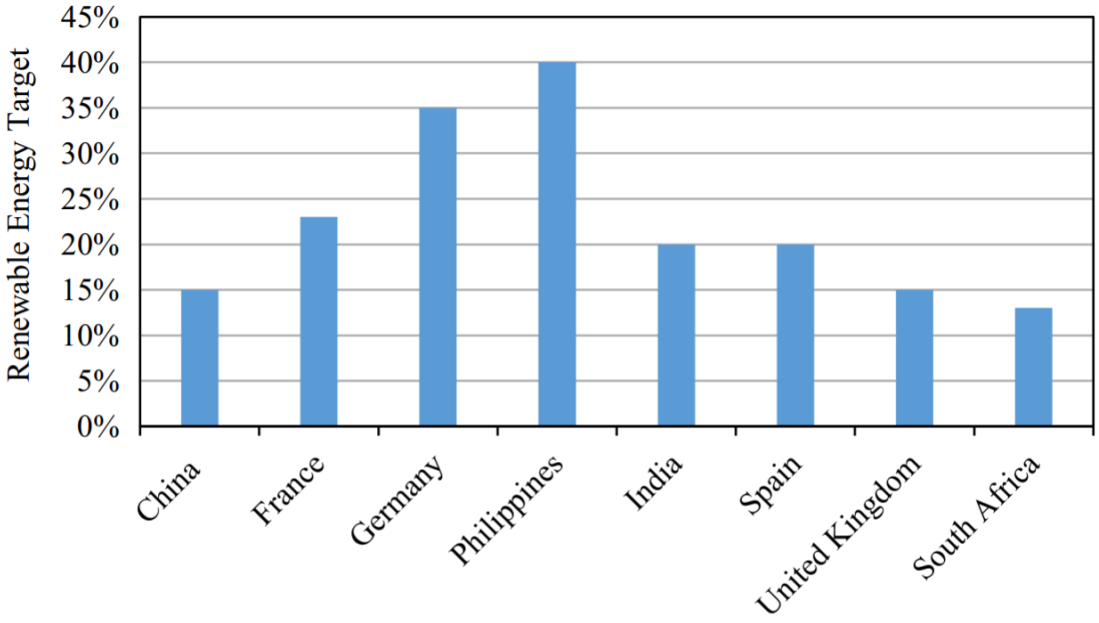

Figure 3:Renewable energy targets by country for 2020

moving towards renewable energy based power generation. Also many countries are introducing more regulations and laws to encourage the power companies to move towards renewable power generation [5][2]. Figure 3 shows the renewable energy targets in 2020 in some countries [12].

In conventional power systems, synchronous generators are being used to generate electrical power from their primary sources of energy such as coal, hydro, oil and nuclear. But, most of the renewable type energy harvesting such as Solar PV and wind involves inverters to integrate them to electrical power system. Moving into more renewable power generation results in converting the generator dominant power system to an inverter dominant power system as illustrated in Figure 4 [13].

Since the world is increasingly progressing towards clean power generation, a lot of inverter dominant power plants are connected to the system. Inverter dominant power plants do not involve any rotational mass; therefore, they do not support the inertia response. It is predicted that with the current rate of increasing the renewable power generation integrating to the grid UK power system will reduce the inertia constant by 70% between 2013/14 and 2033/34 [14][15].

2.5 Drawbacks of Loss of Inertia

Adding more inverter dominant power plants will further reduce the inertia constant of the total system. Having a low inertia constant means, the system has low ability to withstand frequency deviations: with low inertia constant system inertia response will be very poor; therefore, when there is a frequency deviation occurring suddenly, due to poor frequency response against the frequency deviation, frequency can increase or decrease beyond the standard limits. In that case it does not matter how good the primary and the secondary responses are, the system will collapse even before the tertiary response is involved.

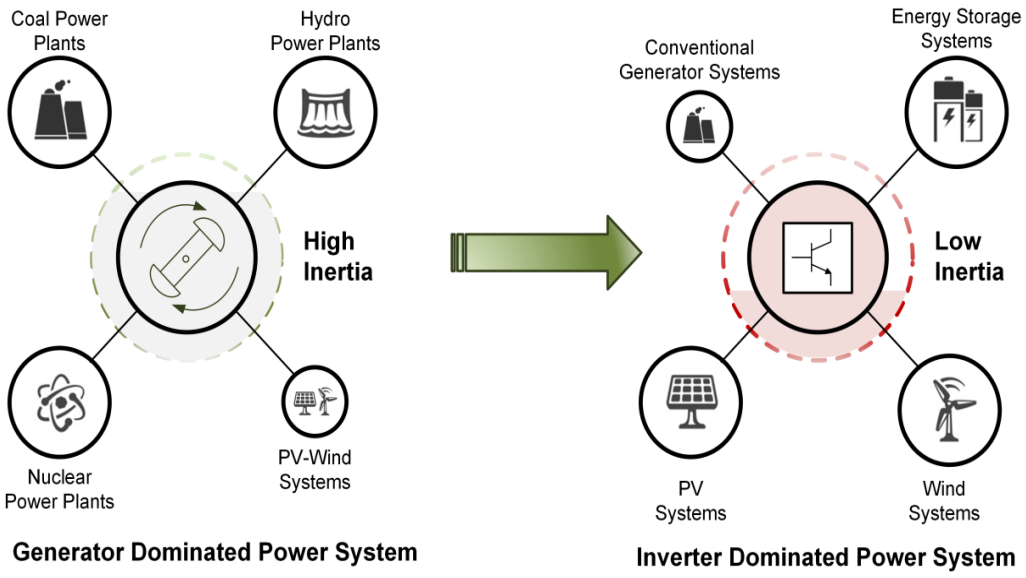

Figure 4:Evolution of the future power system

Therefore, the inertia response is a very important part in a power system. Inertia response is the first line of defence against frequency changes. Also, having a good

inertia response will reduce the amount of deviation of frequency reducing the stress on primary and secondary responses.

2.6 Inertia Emulating Techniques

Concept of virtual inertia was firstly discussed by Prof. Hans-Peter Beck and Ralf Hesse in 2007 [16]. The purpose of virtual synchronous machines is to connect various energy resources for the grid through inverter as synchronous generators as presented in Figure 5.

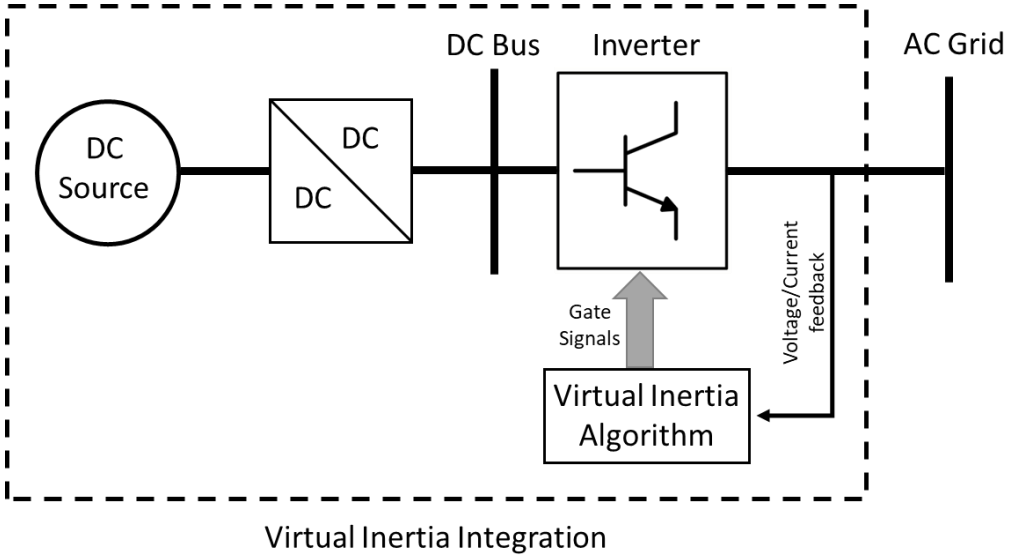

Figure 5:Virtual inertia integration mechanism

There are many virtual inertia topologies available in literature. A brief description of those topologies is described in the following subsections:

2.6.1 Synchronverters

The synchonverter topology emulates the same ideal behaviour of a synchronous generator from the point of view of the grid. This topology targets to integrate renewables without having a major change in the traditional power system. Traditional grid controls can be followed while integrating more inverter dominant power generation.

This was developed in literature by Q.C. Zhong [17]. In that they have modelled nonlinear passive dynamic system without any assumptions on the signals. They have modelled a round rotor machine so the all stator inductances will be constant. Also, this model does not model damper windings. Figure 6 shows the basic controlling of the synchronverter. Since this is not an actual synchronous generator, the moment of inertia (J) and the damping constant (D_P) can be specified independently. Using a phase lock

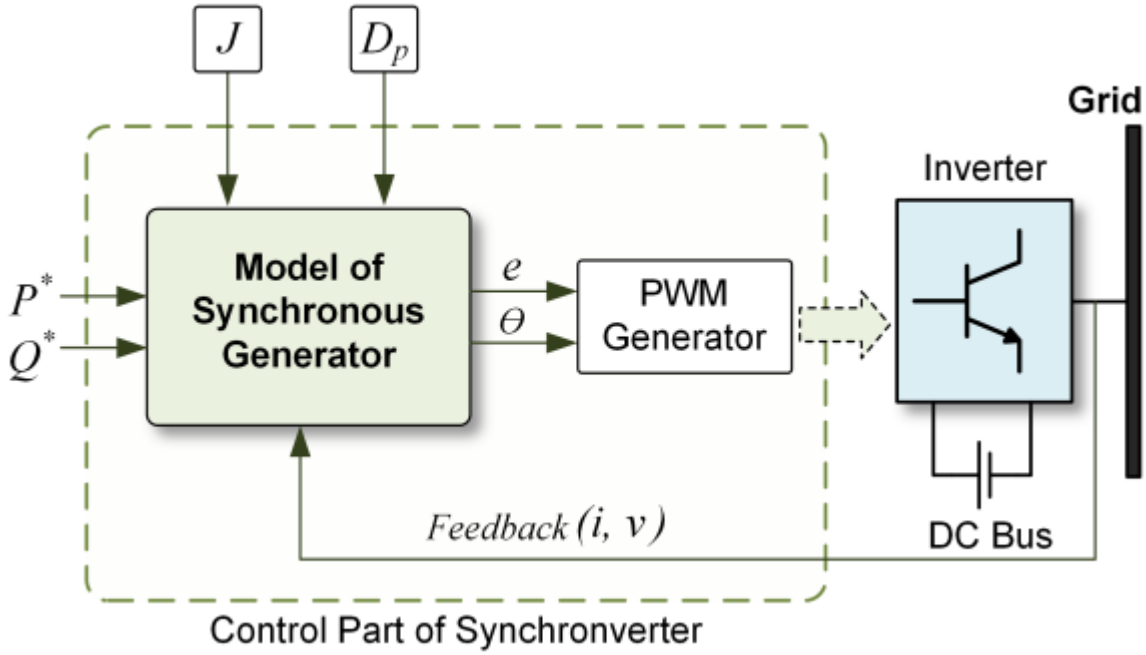

Figure 6:Synchronverter topology

loop (PLL), it is synchronized with the grid. This model works exactly similar to a synchronous generator from the grid point of view.

In literature there are many similar models developed by many researches. They all have modelled the whole synchronous generator with different modelling techniques. Virtual synchronous machine (VISMA) topology [18] Institute of Power Engineering (IEPE) topology [19] and Kawasaki Heavy industries (KHI) lab's topology[20] are some examples for synchronous generator model based virtual inertia implementation.

Since this synchronverter model the exact behaviour of a synchronous generator, it has several complex deferential equations to solve. When solving those complex deferential equations, numerical instability can easily be initiated creating issues in controlling. Requirement of high computational power and lengthy computational time are some drawbacks of the synchronverter topology.

2.6.2 Swing Equation Based

In this topology rather than modelling the exact behaviour of a synchronous generator, the swing equation given in (14) is modelled and solved in each control cycle to emulate the inertia response. This eliminates the complexity of solving differential equations. Therefore, the high computational power requirement is eliminated.

$$P_{in} - P_{out} = J\omega_m \frac{d\Delta\omega_m}{dt} + D_p\Delta\omega \quad (14)$$

$$\Delta\omega = \omega_m - \omega_o \quad (15)$$

Here, J and D_p represent the moment of inertia and damping constant properties respectively, P_{in} is the transferred power to the inverter, P_{out} is the output power from the inverter. ω_m is virtual angular frequency and $\omega_o$is reference angular frequency. Right side of the equation (14) decides whether to supply or absorb active power. The PLL is used to measure the frequency and from that $\Delta\omega$ is calculated. Afterwards,

required power can be supplied or absorbed through the inverter. This emulates the behaviour of the inertia response of an actual synchronous generator. Because of the simplicity and the fast-dynamic response of power electronics, this topology can further improve the inertia response of the system. Depending on the storage capacity, desired J and D_p values can be used. This topology is used in several published research, where different modelling methods are developed based on this concept.

Ise Lab's topology [21] and synchronous power controller (SPC)[22] are some examples using swing equation based modelling techniques in literature. Figure 7 shows the basic block diagram of Ise Lab's architecture [19]. Proper tuning of K_i and K_p is required in this topology. Improper tuning of K_i and K_p can lead to a oscillatory system behaviour[23].

In the swing equation-based topologies published, J and D_p are always kept constant. But, there is an ability to dynamically change J and D_p, because there are virtually emulated properties. Therefore, instead of having fixed J and D_p values, if it is possible to dynamically change those values, a better inertia response can be achieved.

2.6.3 Frequency-Power Response-Based Topology

This is the simplest approach of emulating the inertia. This topology does not incorporate modelling of synchronous generator. This emulates the absorption or release of the active power similar to the way a generator absorbs or releases kinetic energy. Comparing with the traditional droop controller, this topology will provide dynamic frequency regulation. The dynamic control is based on the deviation of the measured frequency and the deviation of the rate of change of the measured frequency. The PLL is used to measure the frequency. Required power ΔP_{VSG} is calculated using equation (16).

$$\Delta P_{VSG} = P_{in} - P_{out} = K_i \frac{d\Delta\omega_m}{dt} + K_p \Delta\omega \tag{16}$$

$$\Delta\omega = \omega_m - \omega_o \tag{17}$$

where K_i and K_p represent the inertia and damping properties respectively. Damping constant helps to regain frequency to its nominal value and reduced the frequency nadir. Inertia constant is breaking the ROCOF by providing dynamic frequency response

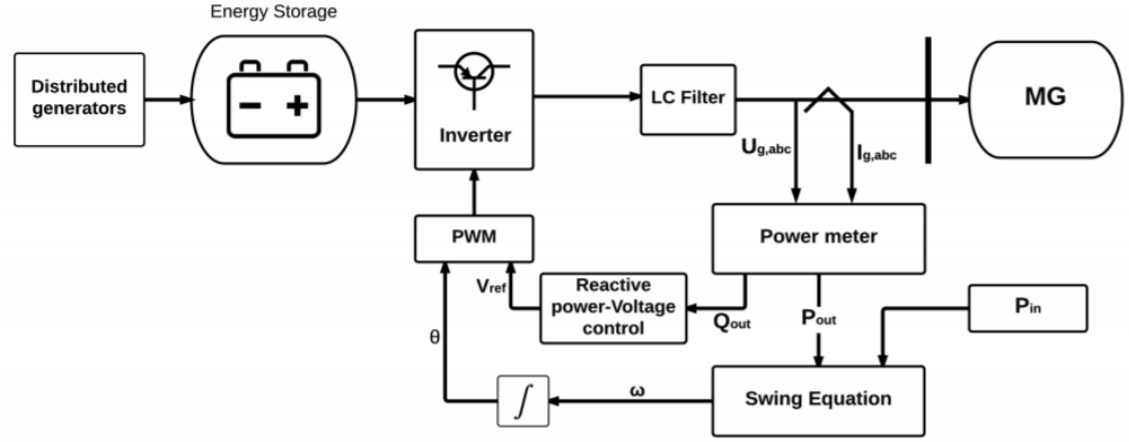

Figure 7: ISE lab's architecture

based on system frequency deviations. This feature is very important in weak grids such as isolated Microgrids. Because of low inertia when there is power mismatch occurs inertial ROCOF is very high. This high ROCOF can trigger the high or under frequency protection relays and system will collapse. VYSNC(a workshop works on renewable energy in Europe) is an example for this topology [24] Figure 8 shows a basic schematic of VYSNC concept.

In this frequency-power based topology K_i and K_p are also kept constant. Since the behaviour of the synchronous generator-based model is used, it is not mandatory to keep K_i and K_p as constants. Having proper controlling techniques, K_i and K_p can be dynamically changed to obtain further improved inertia response.

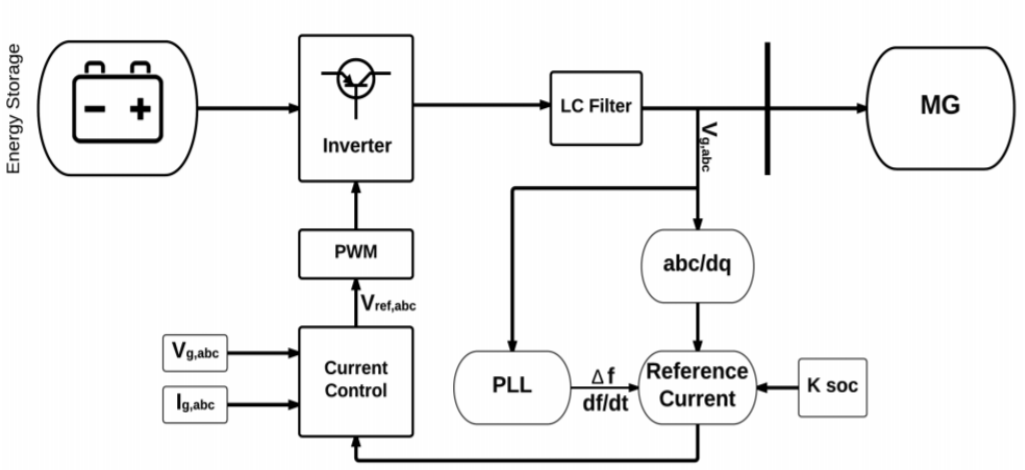

Figure 8:VYSNC architecture

2.6.4 Droop-Based Approaches

Exact or part of the behaviour of synchronous generator is modelled in above discussed methods. But methods like droop based approaches [25][26] doesn't involve modelling the behaviour of synchronous generators. Equation (18) is used to model the droop based approaches.

$$\omega_m = \omega_0 - m_p(P_{out} - P_{in}) \tag{18}$$

Where, ω_m is virtual angular frequency and $\omega_o$is reference angular frequency, $P_{out}$is the measured active power output from the inverter P_{in} is the reference active power and m_p is the active power droop. The schematic of frequency-droop control is shown in Figure 9. Low pass filters are used to measure the exact inverter output filter-out high frequency components which were generated by the inverter. T_f is the time constant of the low passed filter.

Table 3 summarise the above discussed methods of implementing virtual inertia.

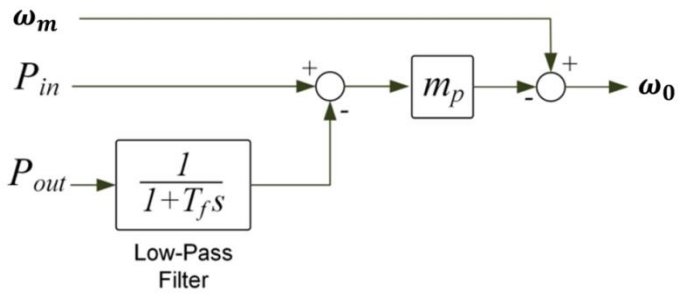

Figure 9: Schematic of frequency droop control

Table 3 : Summary of virtual synchronous machine topologies

Topology	Key Features	Weaknesses
Synchronous generator-based model	Exact replication of conventional synchronous generator behaviour. Grid point of view convention grid structure does not interrupt.	Very high complexity. Slow response. High computation power required. Numerical instability can occur.
Swing equation-based model	Compare with synchronous generator-based model much simple. Less computational power required.	Accurate parameter tuning is compulsory. Otherwise frequency oscillation can occur. Numerical instability can occur.
Frequency-power based model	Straightforward implementation. Simple design	Deviates from exact behaviour of synchronous generator.
Droop based model	Similar to the traditional droop control of synchronous generators. Simplest approach. Very less computational power required. Easy implementation.	Slow transient response. Poor dynamic inertia response support. Deviate from the exact behaviour of synchronous generators.

2.7 Battery selection

In power systems there are various types of energy storage systems required. Due to renewable energy integration, many of these energy storage systems are getting converted from traditional storage systems such as spinning resources to battery-based systems. Depending on the requirement, the features of energy management systems are shown in Table 4.

Table 4: Characteristics of energy storage systems required

		Technical characterises			
Property	**Storage application**	**Power (MW)**	**Back up time**	**Cycles/years**	**Storage response time**
Energy	Spinning resource	~100	Hours	20-50	Sec - minutes
	Load levelling	~100	Hours	250	Minutes
	Black start	~100	Hours	seldom	<1 minute

	Investment deferral	~100	Hours	>100	Minutes
Power	Power regulation with intermitted sources	<10	Minutes	1000	<1minutes
	Integration of non-predictable sources	~10	Minutes	Frequent	<minutes
	Power quality	<1	Minutes	<100	10s- 1 minute
	Line stability	~100	seconds	100	~cycles
	Power oscillating damping	<10	seconds	Frequent	~cycles

Shorter response time and shorter back up time is needed to energy storage systems for reduced the frequency oscillations.

There are 4 basic chemistries used for rechargeable batteries,

1. Lithium-ion (Li-ion)
2. Nickel Cadmium (Ni-Cd)
3. Nickel-Metal Hydride (Ni-MH)
4. Lead-Acid

By comparing the requirements given in the Table 4, Li-ion batteries are the preferable type of batteries for compensating frequency oscillations. In fact, 86% of the energy

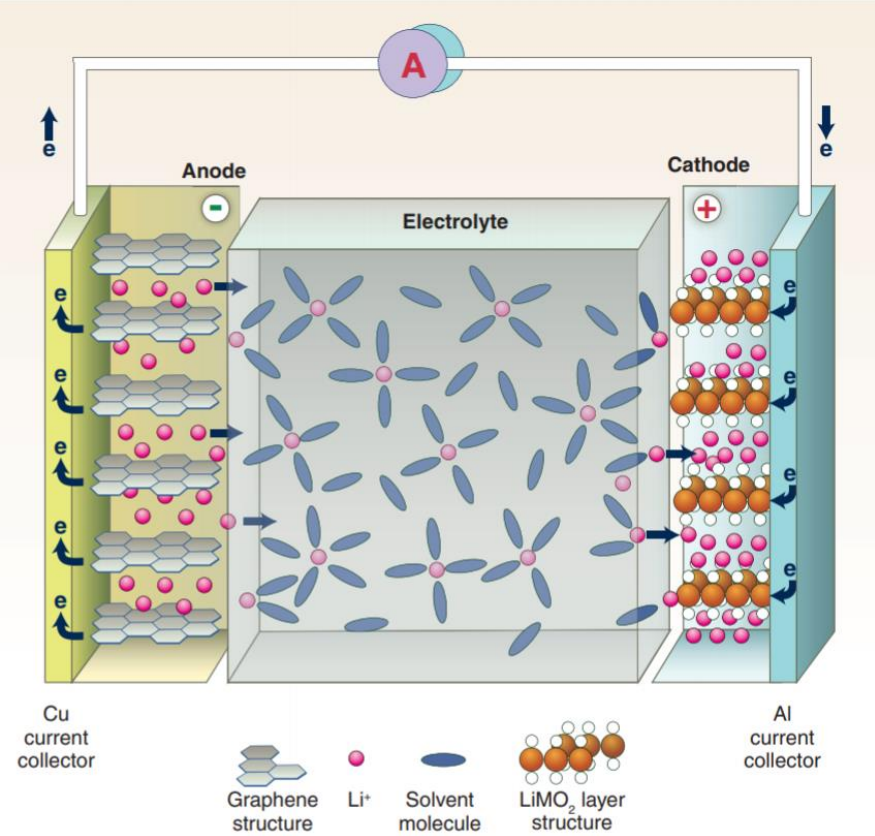

Figure 10: Schematic of Li-ion battery

storage systems worldwide use li-ion batteries [27], because of their energy density, cycle life, fast charge/discharge capability, light weight, and warranties provided by the manufactures. However, the cost of Li-ion batteries are comparatively higher but, with

the mass production, the cost is becoming lower [28]. Because of these features, Li-ion batteries are used in many applications such as for electrical vehicles, solar PV systems and in many electronic devices.

Basic structure of a Li-ion battery is illustrated in Figure 10 [29]. Anode of the Li-ion battery is made from graphite and cathode is made from lithium metal oxide ($LiCoO_2$, $LiMO_2$, $LiNO_2$ etc.). The electrolyte is a solution of lithium salt ($LiPF_6$).

Specification of an industrially applied "Sunrun Brightbox" battery is shown in Table 5 [30].

Table 5: "Sun's Brightbox" Specifications

Total Energy	9.8kWh @25ºC (77ºF)
Usable Energy	9.8kWh @25ºC (77ºF)
Voltage Range (Charge)	400 - 450 VDC
Voltage Range (Discharge)	350 - 430 VDC
Absolute Max. Voltage	520 VDC
Max Charge/Discharge Current	11.9A@420V / 14.3A@350V
Max Charge/Discharge Power	5kW
Peak Power (Only Discharging)	7kW for 10 sec.
Peak Current (Only Discharging)	18.9A@370V for 10 sec. RS485
Communication Interface	RS485
DC Disconnect	Circuit Breaker, 25A, 600V Rating
Connection Method	Spring Type Connector
User Interface	LEDs for Normal and Fault Operation
Protection Features	Over Voltage / Over Current / Short Circuit / Reverse Polarity
Scalability (Total Energy)	Max. 2 in parallel (19.6 kWh@25ºC (77ºF), 6.6KW, 7kW for 10 sec.)

2.8 Microgrids

A microgrid is a group of interconnected loads and distributed energy resources within clearly defined electrical boundaries that acts as a single controllable entity with respect to the grid. A microgrid can connect and disconnect from the grid to enable it to operate in both grid-connected or islanded mode [31]. Most types of renewable power generation such as photovoltaic models, small wind turbines, mini hydro etc. are applied in microgrids. Thus, Microgrids can improve the efficiency and reliability of grid and resolve the energy crisis [32] [33] .

Microgrids can operate in both grid connected and islanded modes. When the microgrid is in grid connected mode, bi-directional power flow between microgrid and the grid occurs. When the microgrid is operating in islanded mode microgrid power generation must meet the demand. Inverter dominant distributed renewable sources contribute in considerable amount of total power generation of the microgrid. Because of that, maintaining microgrid stability is complicated compared to the traditional grid. Depending on the operation method, either grid connected or islanded mode microgrid, stability can be categorized as shown in Figure 11 [34].

Frequency and the voltage of a grid connected microgrid is mainly governed by the utility grid. Therefore, voltage and frequency stability analysis for small size grid connected

microgrids is not essential. But, in islanded microgrids, system stability is mainly governed by the structure of the microgrid. Due to the large capacity of inverter-based power sources in microgrids, microgrids are diverted from the power system traditional controls such as rotor angle control. Loss of distribution generation, short circuit fault and open circuit fault are the main causes for transient stability violations in microgrids [34]. Therefore, microgrid transient stability analyses performed under above conditions.

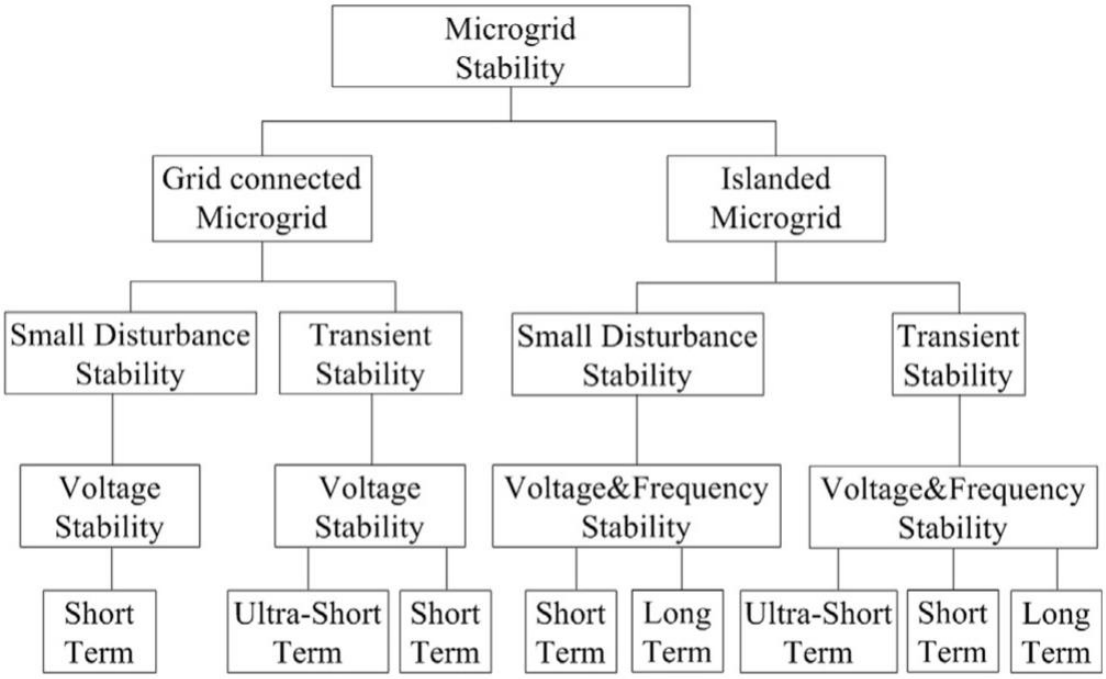

Figure 11: Microgrid stability categorization

Chapter 3: **System design**

3.1 Hydro-PV Microgrid System

Many rural areas use small hydro power plants as their main source of power generation. More than 45,000 small hydro plants have been installed to supply energy for more than million rural population in China[35]. However, the biggest issue with small hydro plants is that it's inability to produced power to match the demand is in dry seasons. To overcome this, most the small hydro based microgrids are integrated with solar PVs to guarantee a reliable power supply throughout of the year. Furthermore, Hydro-PV systems are getting more economically feasible as solar PVs are getting more efficient and less expensive yearly.

Another downside of integrating solar PVs to small hydro-based microgrids is that the reduction of system inertia which leads to a poor inertial response. Therefore, frequency stability of the microgrid under supply demand mismatch will get compromised. This will trigger frequency protection relays and interrupt the electricity supply.

For a hydro-PV system there are 4 main considerations

3.1.1 Electrical Energy Demand

Small hydro generators are the main source of energy whereas solar PVs are used to compensate the energy shortage. Therefore, PV systems should have the capability of delivering the supply demand mismatch during the dry seasons. Furthermore, energy balance must be maintained even in cases of excess generation than demand such as during raining season. Therefore, adding battery energy storage will allow the system to maintain the energy balance in such situations. In summary, microgrids consist of small hydro plants, solar PV and battery energy storage, to improve the reliability of the microgrid.

3.1.2 Peak Power Demand

Small hydro generators cannot run at their rated capacity when the water level is low. Thus, they cannot meet the demand at peak times. Even though solar PVs are integrated to the system, they cannot cater the peak power demand without the rated power from the hydro units. In such situations, battery energy storage should be properly coordinated with PV system to satisfy the demand.

3.1.3 Battery Lifetime

Battery energy storage have to be selected according to the size of the microgird. These batteries should have fast response times to support the microgrid against perturbations, improving the frequency stability. Furthermore, higher number of charging cycles are required. Li-ion batteries have high number of charging/ discharging cycles and it requires less maintenance. Therefore, the life span of the Li-ion batteries is very high.

3.1.4 Generation Cost

A large capacity of the battery energy storage is required in a microgrid. Due to the capital and replacement costs associated with solar and battery energy storage, the generation cost would be higher than that of a conventional system.

3.2 Elements of the Microgrid System

The structure of the microgrid used in this research is shown in Figure 12. This architecture consists of an isochronous generator, solar PV, two batteries and a variable load. This architecture demonstrates the typical behaviour of a Hydro-PV microgrid. Use of two battery energy storage systems has been justified in section 4.4.

3.2.1 Generator Model

A salient pole synchronous generator is used for the hydro power plant. Salient pole synchronous generators are very commonly used in hydro power generation as hydraulic turbines normally operate at low speeds and high torque. Because of low speed operation, generators in hydro plants has a large number of field poles to generate electricity at rated frequency.

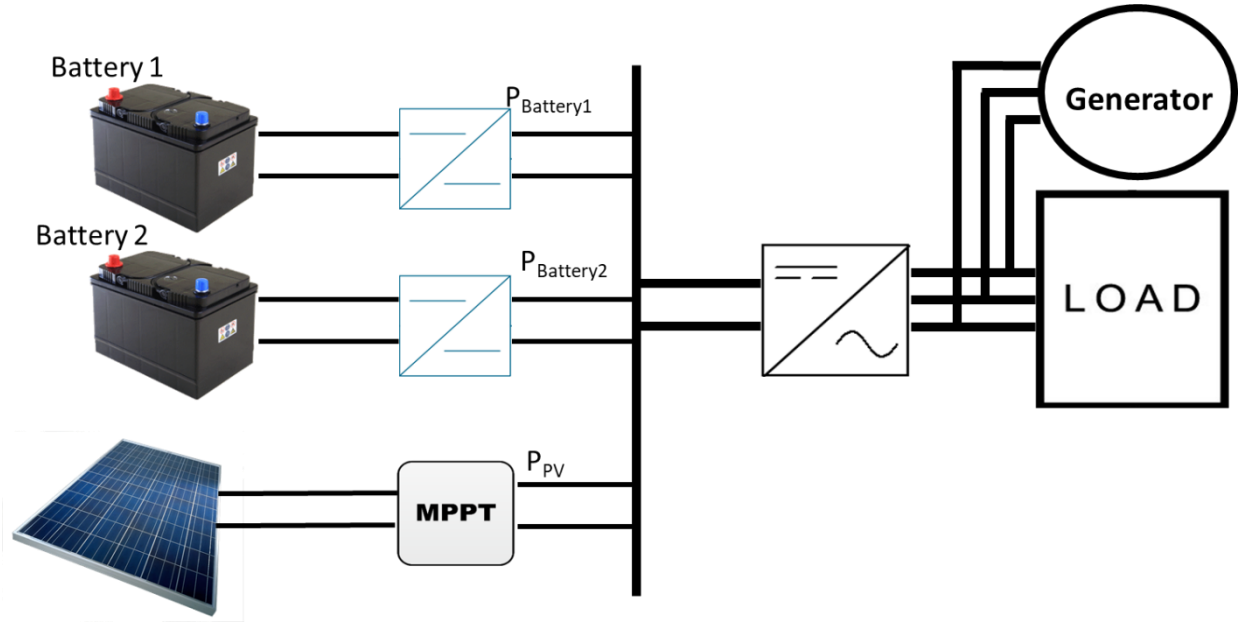

Figure 12: Microgrid architecture

3.2.2 Isochronous Governor

Isochronous governors are suitable when a generator is supplying an isolated load. It cannot be used when there are two or more units connected to the same system. Because each governor has to have precisely the same speed setting. Otherwise, each generator tries to control system frequency according to its own setting.

The speed-droop regulation can be obtained by adding a steady-state feedback loop around the integrator. Control block diagram of an isochronous governor is shown in Figure 13.

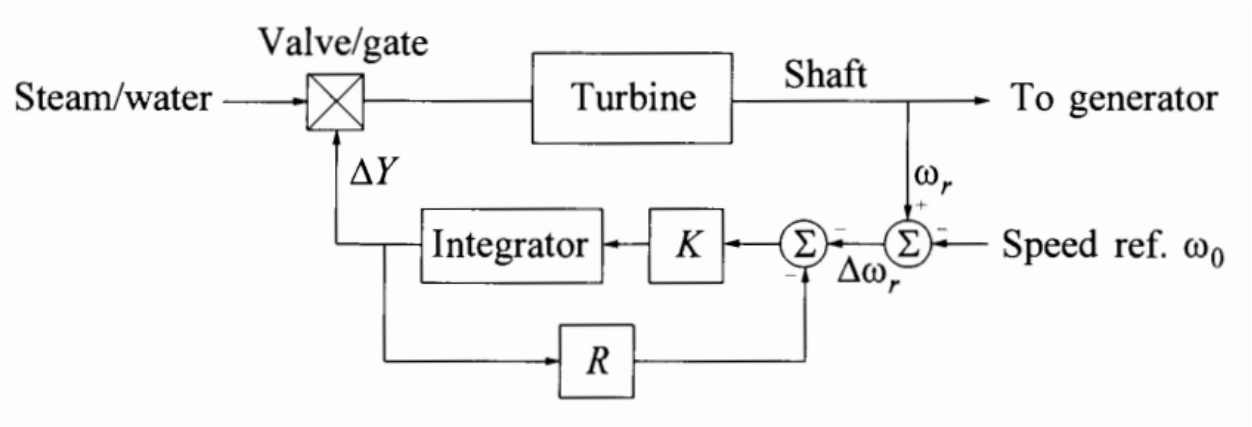

Figure 13: Isochronous governor control

3.2.3 Solar PV

Conventional solar panels are used, and are connected to the inverter through a DC-DC converter which is controlled using the MPPT (Maximum Power Point Tracking) algorithm.

3.2.4 MPPT

This allows to adjust the impedance seen by the solar array to keep the PV system operating at or near the peak power point of the PV panel under varying conditions of solar irradiance and temperature. There are 3 commonly used MPPT algorithms.

3.2.4.1 Perturbation and observation (P&O)

This algorithm changes the operating voltage to ensure operation at the maximum power point, even if the solar irradiance and temperature are constant. This method does not require knowledge of the characteristics of the PV panel and also does not require the measurements of solar irradiance or temperature. Therefore it is easy to implement in both analog and digital circuits [36]. Figure 14 illustrate the P&O algorithm. This method is a widely used MPPT algorithm because of its balance between performance and simplicity. But the drawbacks of this method arelow speed and lack of adaptability, which is needed to track fast transient behaviours under sudden changes in environmental conditions [37]. This method is a simple and straightforward method but due to its slow response, the performance is degraded under sudden changes in the environment.

3.2.4.2 Incremental conductance (IncCond)

The incremental method is based on the principle that the slope of the PV array curve is zero at the maximum power point. So that $^{\Delta P}/_{\Delta V} = 0$, with P=VI.

Considering that

$$\frac{\Delta I}{\Delta V} = -\frac{I}{V} \; if \; P = MPP$$

$$\frac{\Delta I}{\Delta V} > -\frac{I}{V} \; if \; P < MPP$$

$$\frac{\Delta I}{\Delta V} < -\frac{I}{V} \; if \; P > MPP$$

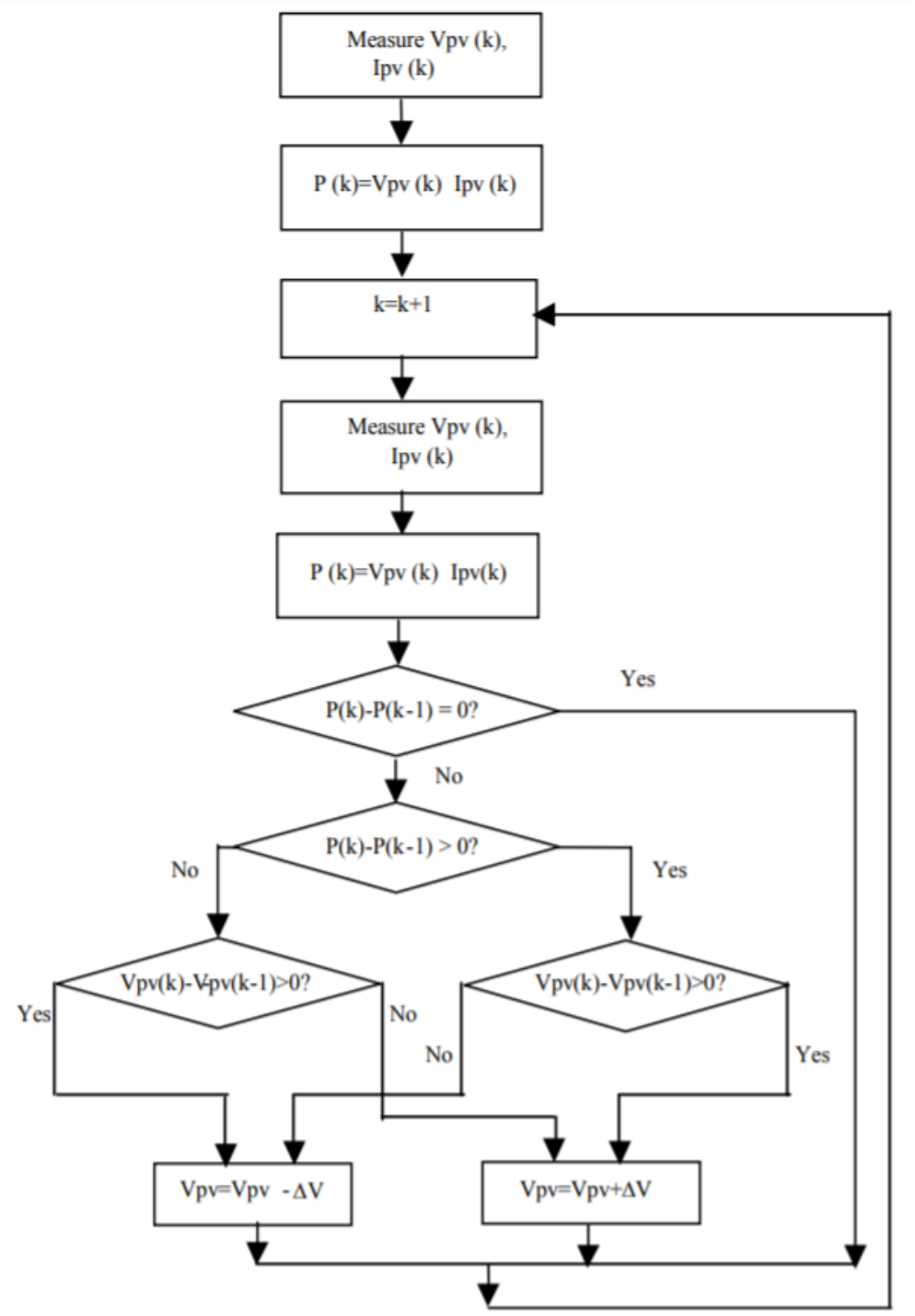

Figure 14: Perturbation and observation algorithm

The MPP can be tracked using the instantaneous conductance $^{I}/_{V}$ with the incremental conductance $^{\Delta I}/_{\Delta V}$. The controller increases or decrease the reference until $^{\Delta I}/_{\Delta V} = -{}^{I}/_{V}$ is achieved. Once the maximum power is reached, the operation of the PV array is maintained at this point. The control algorithm is shown in Figure 15. This is an effective algorithm which needs higher sampling rates and fast calculation capabilities[38]. There are many advantages of this algorithm such as good tracking efficiency and automatic adjustment of the module operating voltage with no oscillations. Control for the extracted power is optimized because of the improved

response [39]. The implementation of this controller is difficult and expensive. But with recent developments in microcontrollers it has become feasible [40].

3.2.4.3 Fractional open-circuit voltage

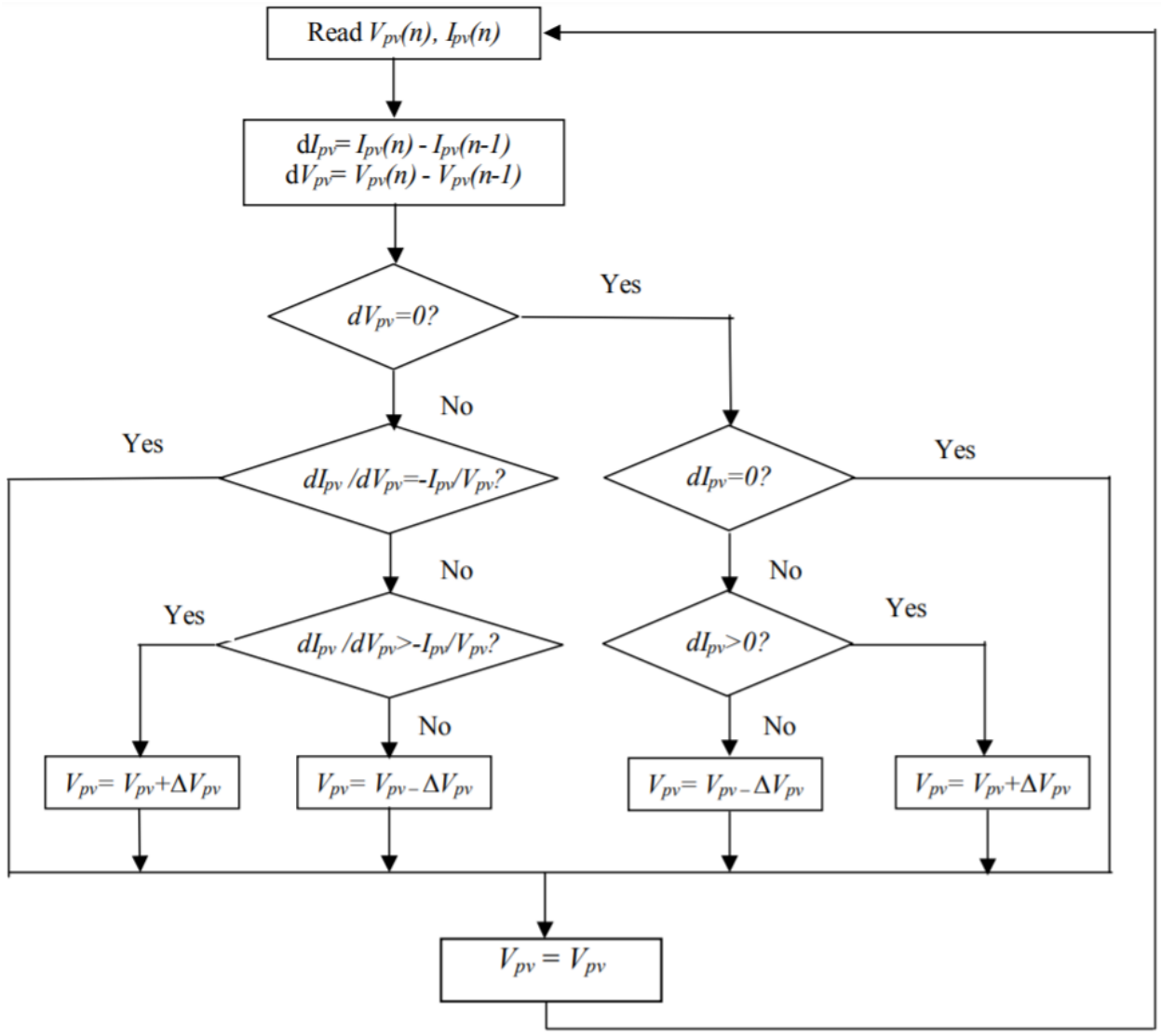

Figure 15: Incremental conductance algorithm

This algorithm is based on the principle that the maximum power point voltage is always a constant fraction of the open circuit voltage. The open circuit voltage of the cells in the photovoltaic array is measured and used as the input to the controller [41].

3.2.5 Variable Load

Microgrids consist of many active loads rather than reactive loads. Variable loads represent two cases.

3.2.5.1 Case 1

Changes in demand side. Connecting a load to the microgrid will increase the total demand on all generators. Whereas, disconnecting a load will reduce the total demand on all generators.

3.2.5.2 Case 2

Changes in generation. The loss of generation from a PV plant is reflected as an increase in load to remaining generators. Excess generation from one PV plant is load reduction by remaining generators.

3.2.6 Battery Energy Storage System

Two battery energy storage systems were used which, are connected to the DC bus through DC-DC battery controllers. These DC-DC controllers control the bidirectional power flow. Thus, they consist of buck-boost converters. Depending on the control signal it works as either a buck or a boost converter and depending on the power reference, charging and discharging rates are determined.

Chapter 4: **Controller Design**

In order to emulate inertia response, two novel controllers were introduced.

1. Virtual Inertia controller
2. Energy Management System controller

4.1 Virtual Inertia Controller

Virtual inertia controller is based on the frequency-power response. The basic principle of the controller is based on equation (19)

$$P_{VSM} = K_I \frac{d(\Delta\omega)}{dt} + K_D(\Delta\omega) \tag{19}$$

$$\Delta\omega = \omega_m - \omega_{ref} \tag{20}$$

P_{VSM} emulate the inertia response of a synchronous generator. $\Delta\omega$ is the system angular frequency deviation, K_I represent the inertia properties of the virtual synchronous generator and K_D represent the damping properties of the synchronous generator, ω_m is the virtual angular frequency and ω_{ref} is the system angular frequency (2π60 rad/s or 2π50 rad/s).

Power supplied or absorb according to the frequency deviation and the ROCOF. Clearly, K_I amplifies the ROCOF negatively. Therefore, P_{VSM} should able to exchange maximum power when the maximum allowable ROCOF occurs. Also K_I should be a negative constant in order to counteract with the polarity of ROCOF.
K_D acts against the frequency change. K_D helps to reinstate the frequency to its nominal value. K_D is also a negative constant.

According to equation (19) and (20), when there is no frequency deviation (Δω=0) P_VSM becomes zero. So, the VSM controller doesn't interact with the normal operation. Therefore, this controller can be integrated into the normal inverter controller and it will be automatically triggered upon the detection of a frequency deviation and switch back to the normal operation when the frequency returns to its nominal value.
In literature K_I and $K_D$calculate using equation (19) and (20) [42].

$$K_I = \frac{P_{VSG\_NOM}}{ROCOF_{MAX}} \tag{21}$$

$$K_D = \frac{P_{VSG\_NOM}}{\Delta\omega_{MAX}} \tag{22}$$

P_{VSG_NOM} is the nominal power rating of the VSM. Literature reports that more effective results can be obtained if the capacity of VSM is selected to be 5% of the total capacity of the microgrid [43].

In this structure, K_I can be changed dynamically as the inertia is implemented virtually. With that inertia response can be given more effectively. As in equation (19) having a

higher K_I value will give more resistance against ROCOF. Even though this will reduce the frequency nadirs, it will take more time to restore to the frequency.

4.2 Stability Criteria with Load Angle Curve

Figure 16 shows the power angle curve of a typical generator. Point A is the original operating point at P1 steady state power. When suddenly a load is connected, power increases to P2 and the new operating point becomes point B.

When the operating point moves along the curve from point A to B, Δω is positive and the machine is in acceleration. As shown in the curve, the new operating point is B. The target is to fix the operating point at B as soon as possible. when the load is connected, the operating point doesn't move to point B right away. Instead, it will go until point C in the first cycle. The time taken to move along the curve from A to B can be reduced by

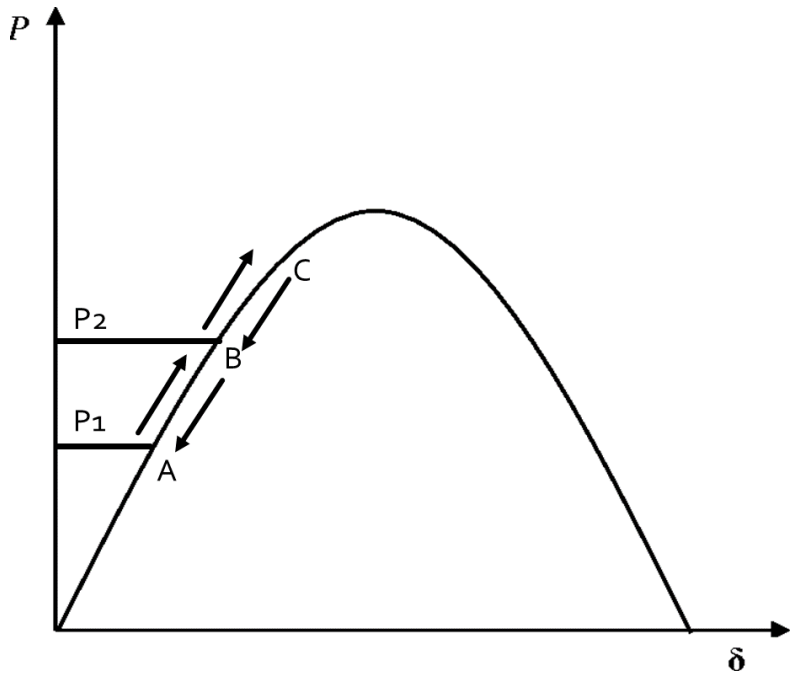

Figure 16: Load angle cure for a sudden demand increase situation

introducing high inertia. High inertia means high kinetic energy. Therefore, time from A to B can be made much shorter by releasing the required amount of kinetic energy. From B to C along the curve, Δω is still positive but the machine is on deceleration mode. Having higher inertia will not help in this situation. Higher inertia will take point C further away from point B. For this situation, low inertia will effectively reduce the length between B and C in the curve (point C gets much closer to point B). From C to B along the curve, Δω is negative but the machine is in acceleration mode. Thus, inertia has to be increased to reduce the time from C to B. After it pass the point B, again Δω is negative and the machine is in a deceleration mode and having a low inertia will help in this part. Low inertia will reduce the amount it deviates from the point B. Thus, having an alternating inertia will make the response much faster and smoother.

However, it is not be feasible to implement the above mechanism in conventional generators, because connecting and disconnecting masses is not efficient and practical. But it is possible with the concept of virtual inertia. Each and every operating region

needs to be identified precisely in order to implement the above controller. The Identification of regions can be easily done using with Δω and ROCOF. Table 6 summarizes the identification method of the areas in the power angle curve using the direction of Δω and ROCOF. After identifying each section, alternating inertia constant (KI) can be assigned to the corresponding section.

Table 6: Identification of different regions in the load angle curve

Segment	Δω	$\frac{d\omega}{dt}$	Mode	KI
A to B	>0	>0	Acceleration	High
B to C	>0	<0	Deceleration	Low
C to B	<0	>0	Acceleration	High
B to A	<0	<0	Deceleration	Low

4.2.1 Variable Inertia Constant Controller

System frequency is measured using a PLL. As shown in Figure 17, frequency deviation is calculated by comparing the measured frequency with the reference frequency. which is then multiplied by 2π in order to calculate the angular frequency deviation. Then the ROCOF is calculated from taking the derivative of the change in angular frequency.

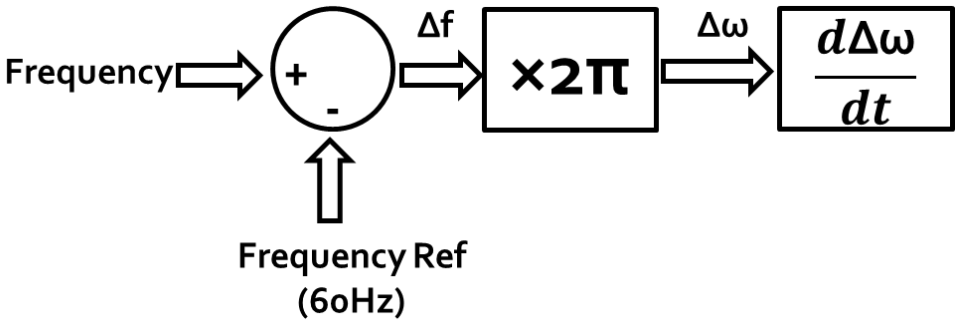

Figure 17: Δω and ROCOF calculation controller

The process of the variable inertia constant controller action is shown in Figure 18. The polarity of the deviation in angular frequency (Δω) is identified first and is followed by a polarity check of the ROCOF.

If $\Delta\omega > 0$ and $^{d\omega}/_{dt} > 0$ then higher inertia constant is assigned
If $\Delta\omega > 0$ and $^{d\omega}/_{dt} < 0$ then lower inertia constant is assigned
If $\Delta\omega < 0$ and $^{d\omega}/_{dt} > 0$ then higher inertia constant is assigned
If $\Delta\omega < 0$ and $^{d\omega}/_{dt} < 0$ then lower inertia constant is assigned

Having multiple inertia constants is not effective in the transient stage as it is important to have a quick and sharp response. Having a multiple step wise inertia constant in increments and decrements will not give a quick and sharp response but will slow down

the response. Therefore the best option is to have only two stages to the inertia constant, which is the lowest and the highest value of inertia constant.
lowest and the highest value of inertia constant .

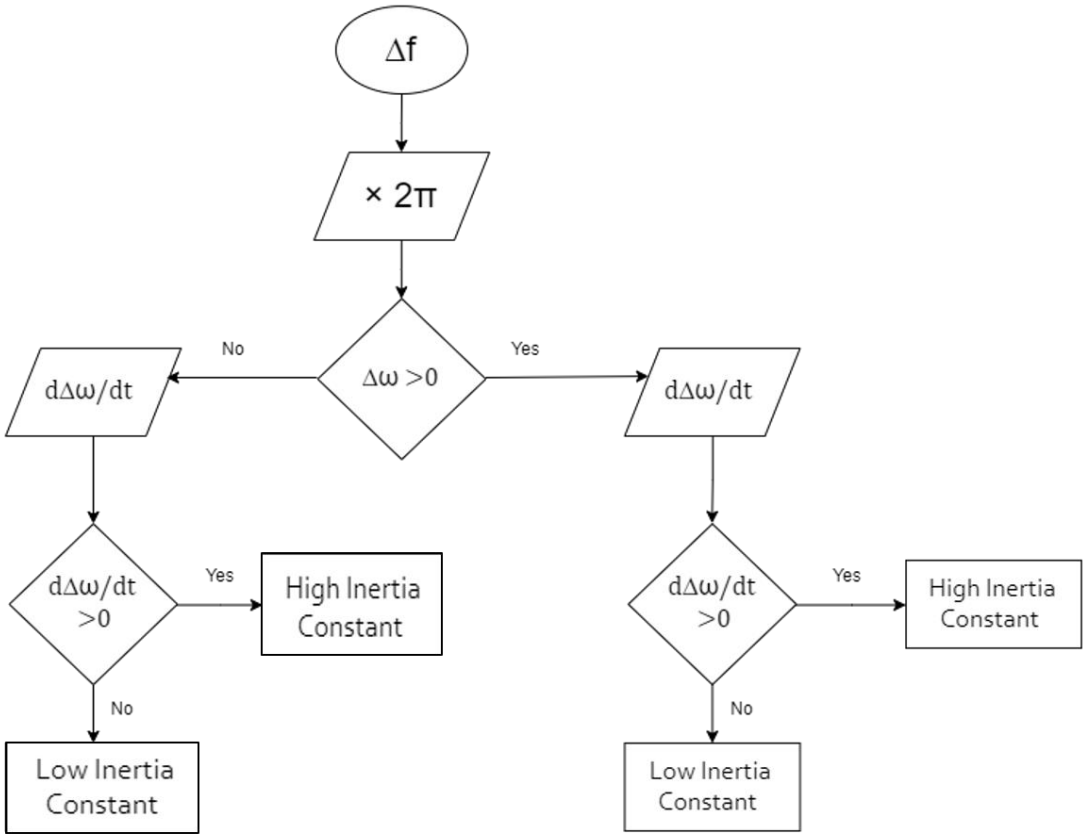

Figure 18: Variable inertia constant controller

4.3 Virtual Inertia Constant Controller Implementation

Equation (19) is modelled in the controller as shown in Figure 19. Inertia constant is fed from the variable inertia constant controller. Deviation of angular frequency is multiplied from the damping constant and added to the product of the variable inertia constant and the derivative of the angular frequency deviation. This will generate the required active power that needs to be exchanged between the inverter and the

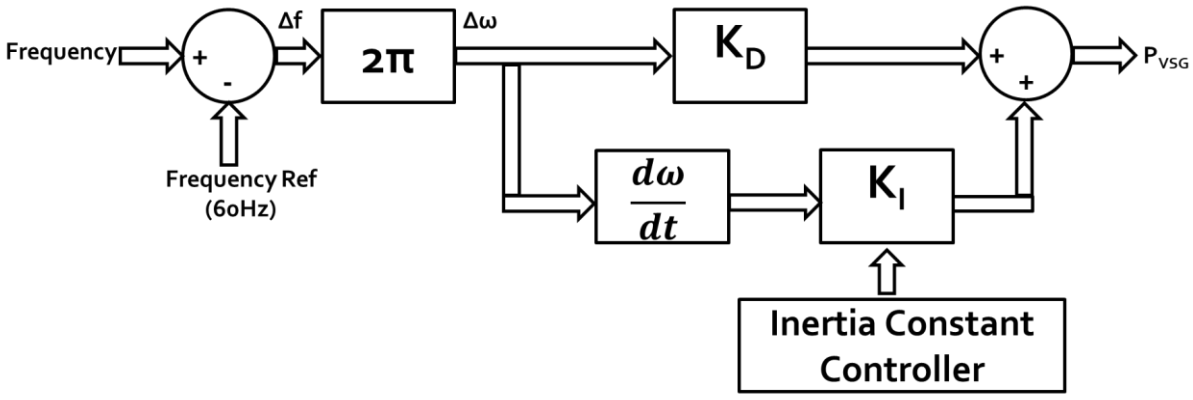

Figure 19: Virtual inertia controller

microgrid to enhance the inertia support. P_{VSG} is the active power reference to the inverter.

4.3.1 Current Controller

Current controller will produce a current reference based on the active power reference produced by the virtual inertial controller. linear current controller in Direct-quadrature(d-q) based rotating frame is used as sown in Figure 20 [44]. The direct component of the current reference is formulated by the power reference using equation (23).

$$I_d^* = \frac{2}{3}\left(\frac{V_d P_{VSG} - V_q Q}{V_d^2 + V_q^2}\right) \quad (23)$$

$$I_q^* = 0 \quad (24)$$

Where I_d^* and I_q^* are d and q axis requird current components of the inverter respectively, V_d and V_q are d and q components of the grid voltage respectively and Q is the reactive power reference. Reactive power reference is set to zero as active power is the only interest for the inertial response. PI controller drives the steady state error of d-q current components to zero. D-q components of the reference grid voltage is generated by comparing the reference d-q current with the measure d-q current. Then, in the secondary control loop from the equation (25) is used to calculate the d-q axis voltage references.

$$\begin{vmatrix} V_d \\ V_q \end{vmatrix} = L\frac{d}{dt}\begin{bmatrix} i_d \\ i_q \end{bmatrix} + R\begin{bmatrix} i_d \\ i_q \end{bmatrix} + \omega L\begin{bmatrix} -i_q \\ i_d \end{bmatrix} + R\begin{bmatrix} e_d \\ e_q \end{bmatrix} \quad (25)$$

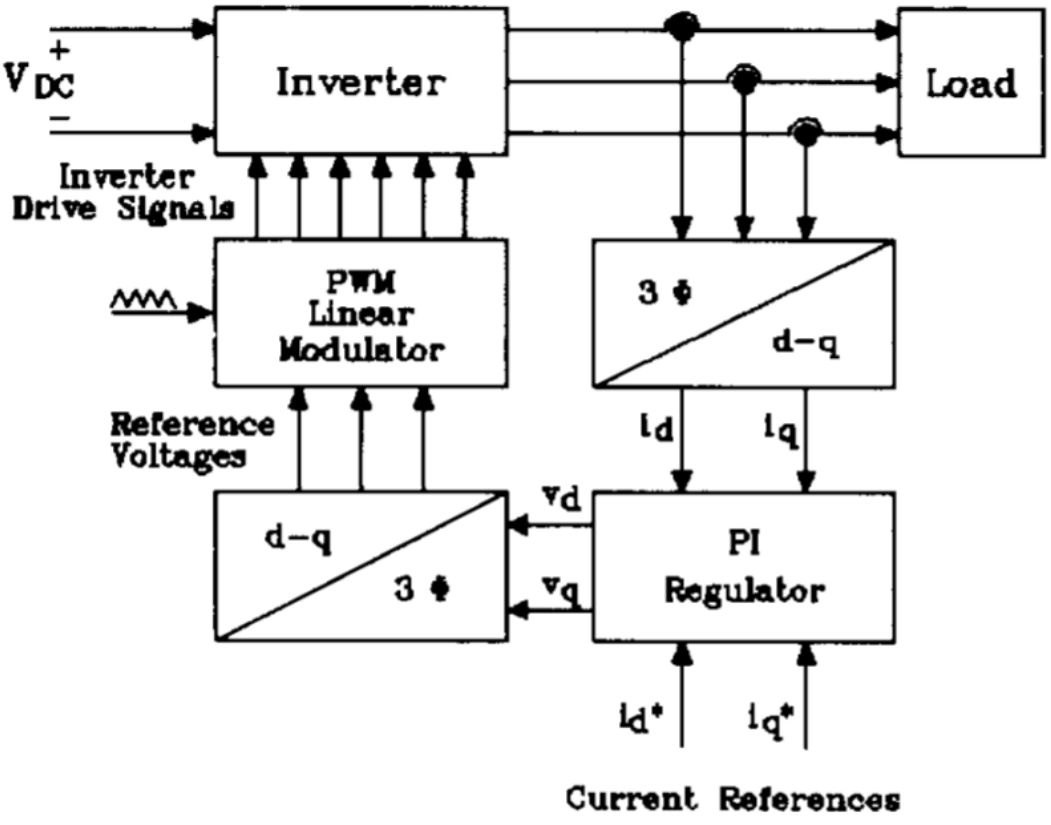

Figure 20: Rotating frame linear current regulator

4.3.2 Inverter Controller

Grid-injecting mode control is used in the inverter. This technique is used when the inverter is connected to the grid after successful synchronization. This mode will allow the grid-connected inverter to be operated at a controlled power output to the Microgrid. This setup will generate output power which follows the desired power reference. Figure 21[45] shows a complete block diagram of a grid-injected inverter control.

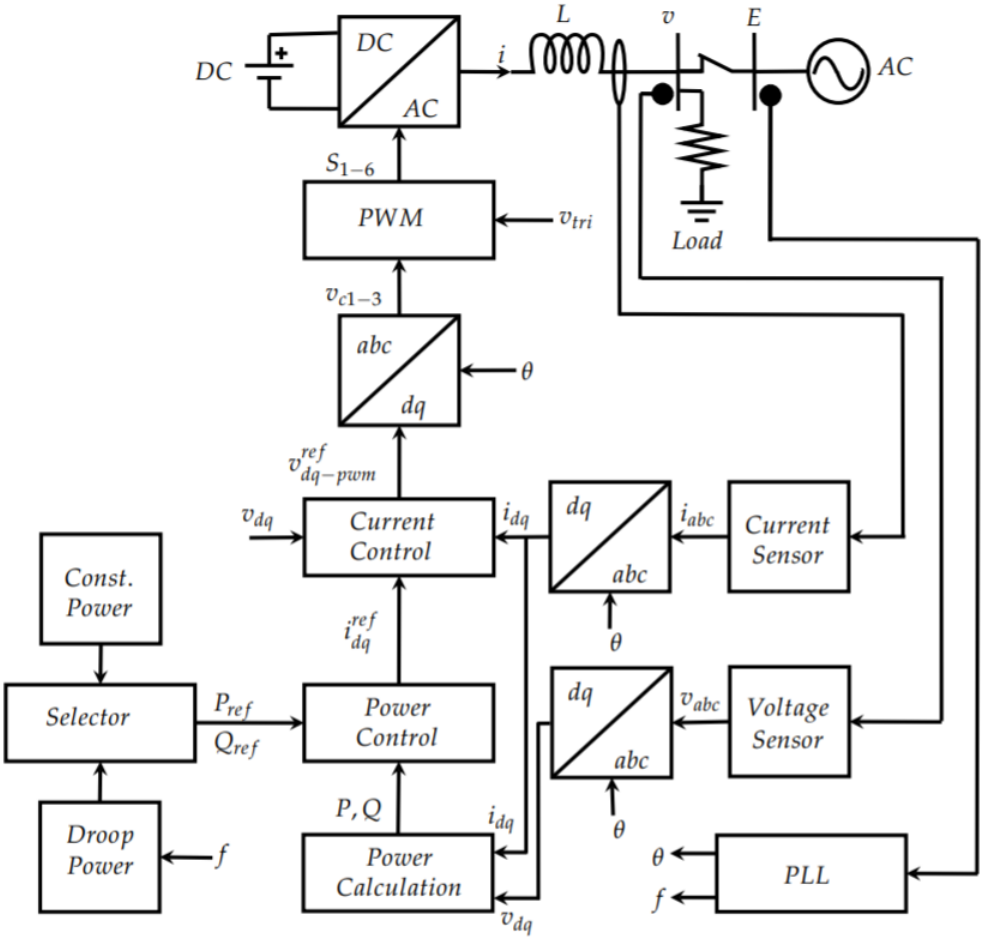

Figure 21: Grid-Injecting Mode Control for the inverter

4.3.3 Overall Inverter Control

Overall inverter controller is shown in Figure 22. The synchronization angle Θ from PLL is used to decouple the grid voltage and the current components into d-q components. I_d and I_q values are calculated using equation (19). P_{VSG} is calculated using the VSG controlling algorithm. Then calculated I_d and I_q values are compared with d-q components of measured inverter output current and generate the reference d-q frame current components of the inverter which are $I_{D\,ref}$ and $I_{Q\,ref.}$. D-q axis voltage references are calculated using the equation 25. Using the synchronization angle Θ, d-q components are coupled back to produce the three phase reference voltages which are compared against a high frequency triangular waveform to produce Pulse Width Modulated (PWM) signals to MOSFETs in the inverter.

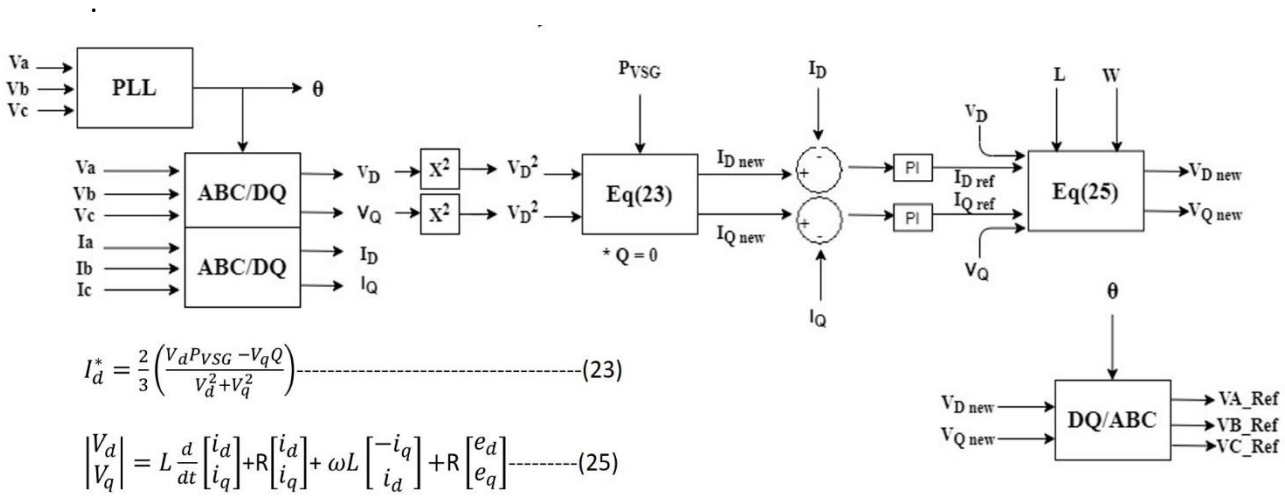

$$I_d^* = \frac{2}{3}\left(\frac{V_d P_{VSG} - V_q Q}{V_d^2 + V_q^2}\right) \text{----------(23)}$$

$$\begin{vmatrix} V_d \\ V_q \end{vmatrix} = L\frac{d}{dt}\begin{bmatrix} i_d \\ i_q \end{bmatrix} + R\begin{bmatrix} i_d \\ i_q \end{bmatrix} + \omega L\begin{bmatrix} -i_q \\ i_d \end{bmatrix} + R\begin{bmatrix} e_d \\ e_q \end{bmatrix} \text{---------(25)}$$

Figure 22: Inverter overall control

4.4 Energy Management System (EMS)

As shown in Figure 23, EMS takes inputs: PVSG generated from the VSM controller and power measurement from the PV system which produces two control signals for each battery controller. Battery controllers will control the power exchange between battery and the DC link. EMS contains two sets of batteries and separate controllers for each battery. The purpose of this design is to enhanse the response time. Suppose there is a situation that needs to change the operation status from charging to discharging state immediately. In such a situation, if only one battery is used, the battery needs to be changed immediately from charging mode to discharging mode. This sudden change of states will introduce unwanted transients and is harmful for the battery lifetime. By introducing two batteries such situations can be avoided as while one battery is on the charging mode other battery can be set to discharging configuration. When the change of states is required, charging battery can be switched off and the discharging battery can be switched on. This will eliminate unwanted transients, and will not damage batteries.

4.4.1 Battery Controller

Battery controller consist of two control strategies.

1. Upper level control: Select the on/off condition of the battery and select the operation mode charge/discharge.
2. Lower level control: Decide the rate of discharge/charge.

When the grid frequency is higher than the rated value (demand is lower than the generation), energy needs to be absorbed by the VSM. Batteries are the only device in VSM which can absorb energy. Thus, batteries must have sufficient storage capacity available to store energy. Therefore, state of charge (SOC) of the batteries are kept at 70%. Remaining 30% of each battery is reserved to absorb energy whenever necessary.

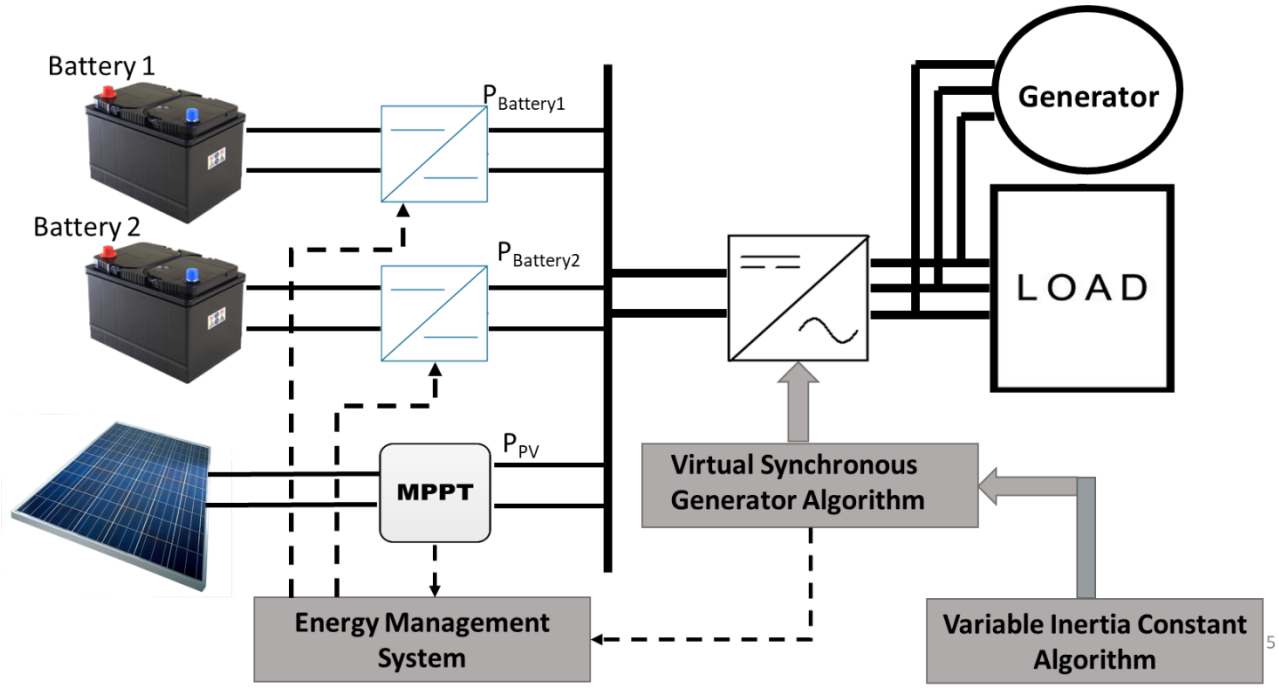

Figure 24: Energy Management System

EMS incorporation to the microgrid is shown in Figure 24. It first checks the frequency from PLL and if the grid frequency is higher than the 60Hz (demand is less than the generation), both batteries will go to charging mode and the power that needs to be absorbed is given from the equation 26. This controller will allow the MPPT to continue operating. Generated power from the solar PV will be directed to batteries. When the frequency fluctuation is stabilized stored power will release gradually until the SOC of the batteries reach 70%.

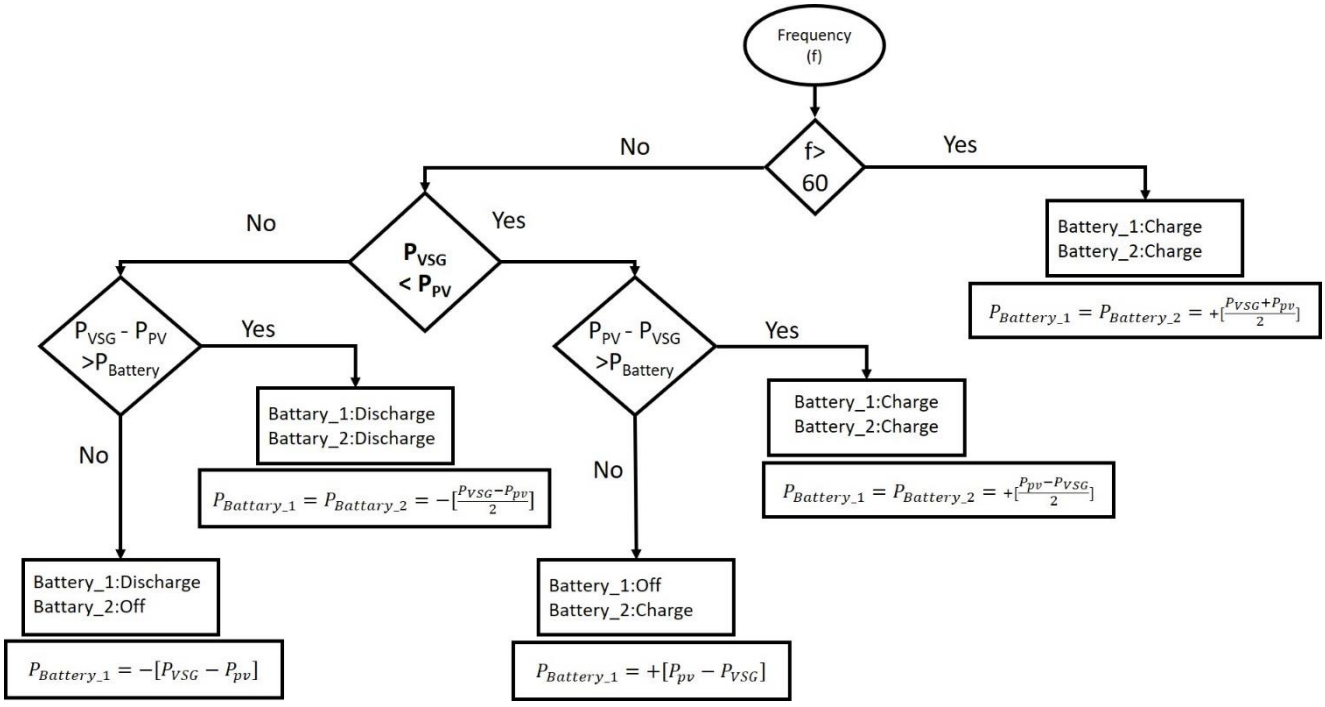

Figure 23: Battery controller

$$P_{Battery\_1} = P_{Battery\_2} = +[\frac{P_{VSG}+P_{pv}}{2}] \quad (26)$$

When the frequency is less than 60Hz (demand is higher than the supply). VSM have to inject the power in order to emulate the inertia response. Since the solar PV is also providing the power to the grid, P_{VSM} is compared with the P_{PV} (power produced by the solar PV). Since two-battery setups are being used, controller checks whether the required power can be given from one battery. If so, the controller will force one battery to be discharged. If one battery is not sufficient, both batteries will be forced to enter the discharging mode.

If the power requirement is higher than the power generated by the solar PV and the required additional power is less than the power of a single battery, one battery will discharge, and the other battery will be turned off. Power reference for the battery is given by equation 27.

$$P_{Battery\_1} = -[P_{VSG} - P_{pv}] \quad (27)$$

If the power requirement is higher than the power generated by the solar PV and the required additional power is higher than the power of a single battery, both batteries will be discharged. Require power for each battery is given by equation 28.

$$P_{Battery\_1} = P_{Battery\_2} = -[\frac{P_{VSG}-P_{pv}}{2}] \quad (28)$$

If the power requirement is less than the power generated by the solar PV and the required additional power is less than the power of a single battery, one battery will be discharged, and the other battery will be turned off. Power reference for the battery is given by equation 29.

$$P_{Battery\_1} = +[P_{pv} - P_{VSG}] \quad (29)$$

If the power requirement is less than the power generated by the solar PV and the required additional power is higher than the power of a single battery, both batteries will be discharged. Required power for each battery is given by equation 30.

$$P_{Battery\_1} = P_{Battery\_2} = +[\frac{P_{pv}-P_{VSG}}{2}] \quad (30)$$

Chapter 5: **Simulated Model**

Simulation model consists of a synchronous generator, Solar PV plant, batteries storage and two loads shown in the Figure 25. Those loads are modelled as constant active power loads. One of the loads is connected through a circuit breaker to allow. Sudden connection/disconnection which can represent demand mismatch. It can represent supply demand mismatch either from the generation side or from demand side. PV –

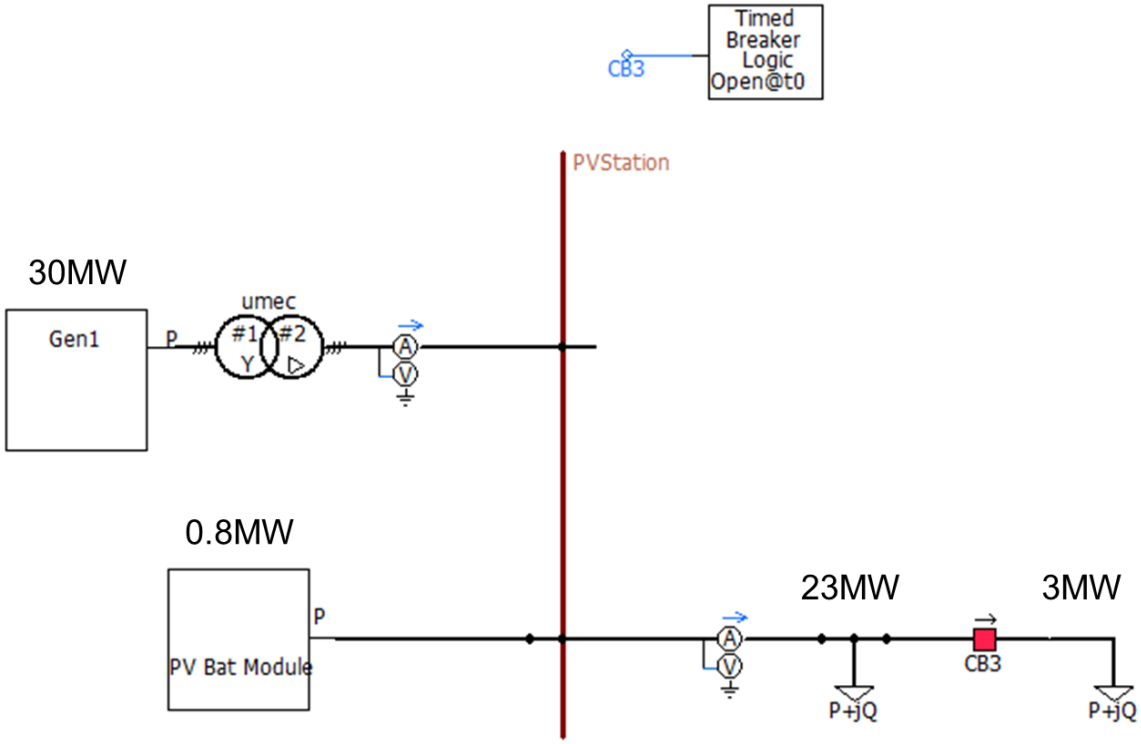

Figure 25: Simulation model

Battery model consist of two batteries along with two DC-DC controllers. Batteries and solar PVs are connected to a single DC link which then connects to the inverter and the inverter to the ac lines in the microgrid as shown in Figure 26. Table 7 shows capacities of each component in the microgrid.

Table 7 : Capacity of the each component in Microgrid

Component	Capacity (MW)
Synchronous Generator	30
Solar PV	0.25
Battery 1	0.6
Battery 2	0.6
Fixed load	23
Load connected through circuit breaker	3

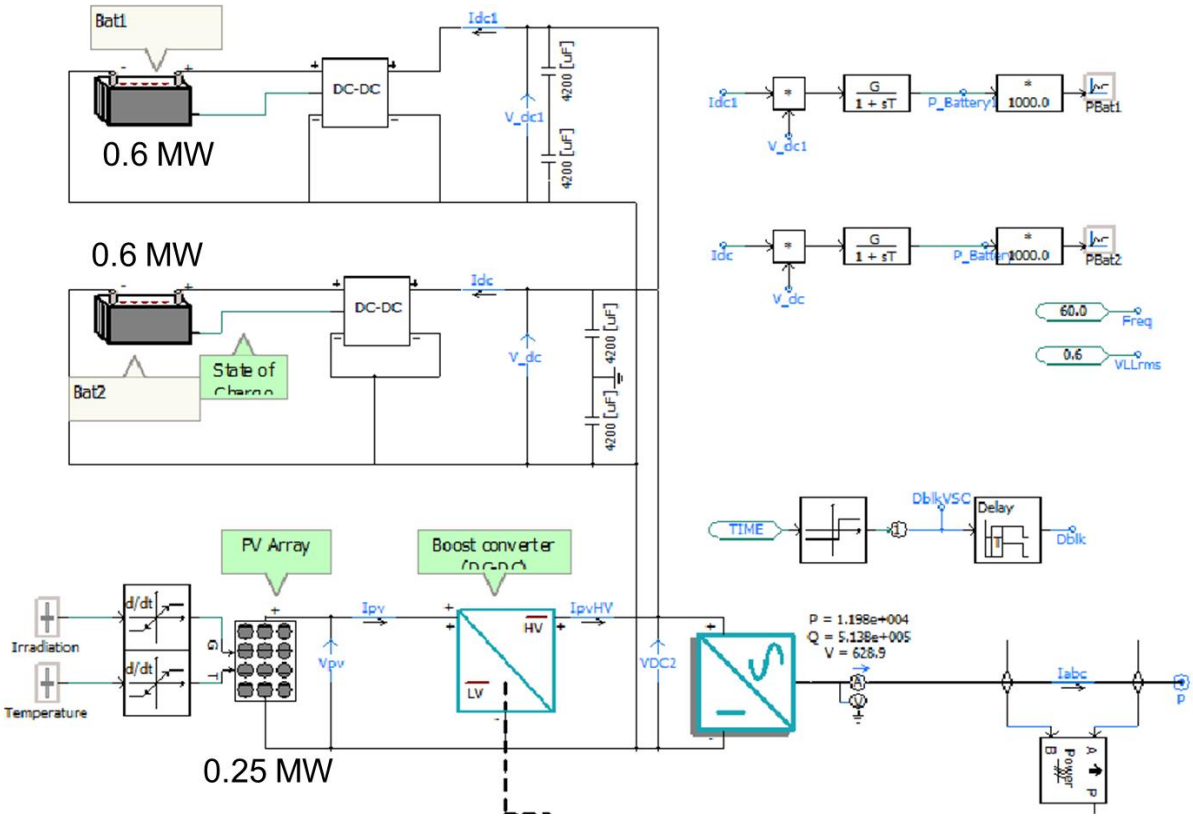

Figure 26: PV Battery model

5.1 PSCAD™/EMTDC™

PSCAD offers to build, simulate, and model systems easily, providing limitless possibilities in power system simulations. It has comprehensive library with wide range of models which are used in control systems, electric machines and power systems. PSCAD has been used for simulations for more than 40 years by researchers. PSCAD enables practicing engineers and researchers to design, analyse, optimize and verify their designs. PSCAD has become the most popular power system transient simulation package available today.

PSCAD is the most suitable for simulating electromagnetic transients and it's simulation speed is very high compared to other simulation softwares. Due to its large component library and user-friendly interface, it allows the user to analyse more comprehensive circuits accurately and easily. Therefore, simulations of this research were carried out using PSCAD software.

5.2 Synchronous Generator

PSCAD generator model provides an option to model a salient-pole machine or a round-rotor machine. This configuration is obtained in PSCAD by varying the number of Q-axis damper winding as shown in Table 8.

Table 8 : Generator selection criteria in PSCAD

Machine Type	Number of Q-axis damper
Salient-pole machine	1
Round-rotor machine	2

There are many advanced options can be specified in the synchronous machine model in PSCAD. But for a general default parameter can be used. Purpose of these advanced parameters are to mainly initialize the simulation and to reach desired steady sate as soon as possible. Appendix A presented the parameters of the synchronous generator model.

Steady state conditions are obtained from a load flow analysis. Once the steady state is reached, disturbances can be applied to observe the transient response.

5.2.1 Exciter

Exciters are modelled in PSCAD as dynamic transfer functions and it can be interfaced directly to the synchronous machine model. Several pre-defined exciter modules available in PSCAD master library. AC excitor systems used in PSCAD consist of an alternator and either stationary or rotating rectifiers to produce the direct current for the synchronous machine field. A standard IEEE type exciter AC1A, is selected in this study.

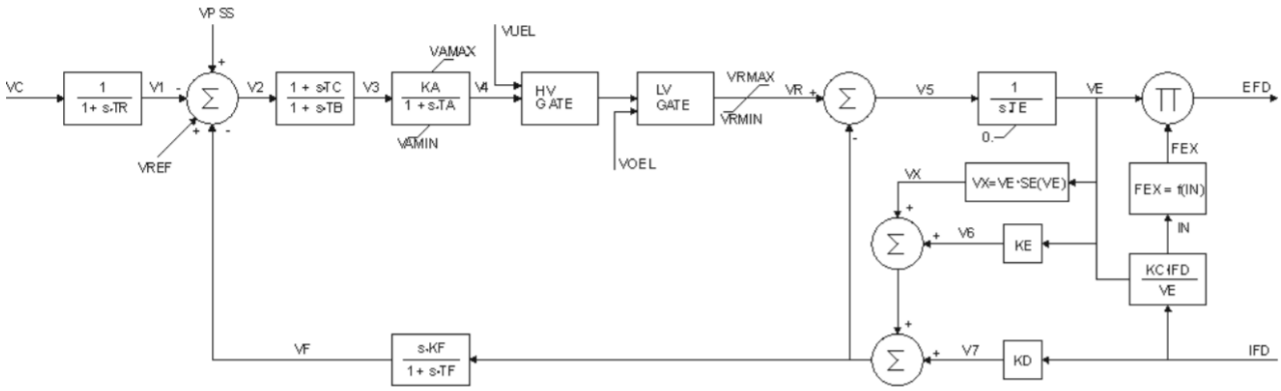

Figure 29: Block diagram of the AC1A exciter

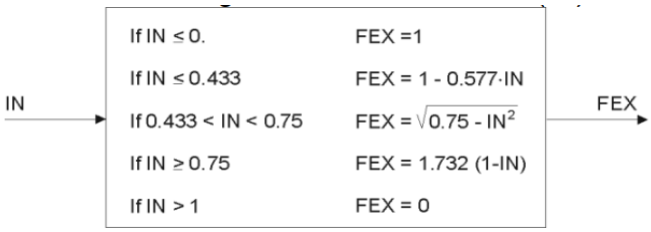

Figure 28: The Rectifier Regulation Characteristic F(IN)

5.2.2 IEEE type AC1A Exciter Model

This type of exciter does not employ self-excitation. Power to voltage regulation is taken from a source which is not affected by external transients. The diode characteristics in the exciter output imposes a lower limit of zero on the exciter output voltage[46]. Block

diagram of an AC1A exciter and the rectifier regulation is shown Figure 27 [47] and 28 respectively. Table 9 contains the parameters of the block diagram shown in Figure 27 and 28.

Table 9 : Parameters of IEEE type AC1A excitor

NAME	Type	Description
TR	Seconds	Filter time constant
TB	Seconds	Voltage regulator time constant
TC	Seconds	Voltage regulator time constant
KA	pu	Voltage regulator gain
TA	Seconds	Maximum voltage regulator output
VAMAX	pu	Minimum voltage regulator output
VAMIN	pu	Minimum voltage regulator output
TE	Seconds	Exciter time constant, integration rate associated with exciter
KF	pu	control
TF	Seconds	Excitation control system stabilizer gains
KC	pu	Excitation control system stabilizer time constant
KD	pu	Rectifier loading factor proportional to commutating reactance
KE	pu	Demagnetizing factor, a function of exciter alternator
E1	pu	reactance
SE1	pu	Exciter constant related to self-excited field
E2	pu	Exciter alternator output voltages back of commutating
KF2	pu	Coefficient to allow different usage of the model. Typical Value=1
HVLVGATES	Boolean	Indicates if both HV gate and LV gate are active (HVLVgates). true = gates are used false = gates are not used. Typical Value = true.

5.2.3 Hydro Turbine

A standard IEEE type hydro turbine provided in the PSCAD library was used in the study. Default parameters were used for the hydro turbine unit. Parameters for simulated hydro turbine given in Appendix B.

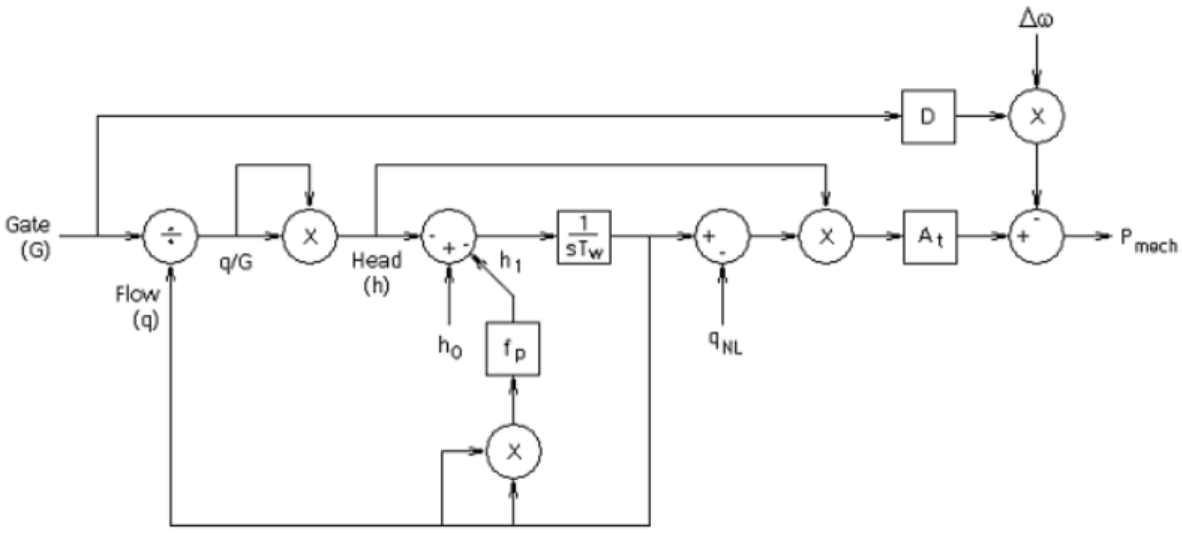

Figure 30: Turbine transfer function

Transfer function of the turbine is illustrated in Figure 29 [48]. A_t is the turbine gain factor flow, f_p is the penstock head lost coefficient, G is the gate position, q is the turbine flow before reduction by deflector and relief valves, q_{NL} is the no load water flow and T_w is the starting time.

5.2.4 Hydro Governor

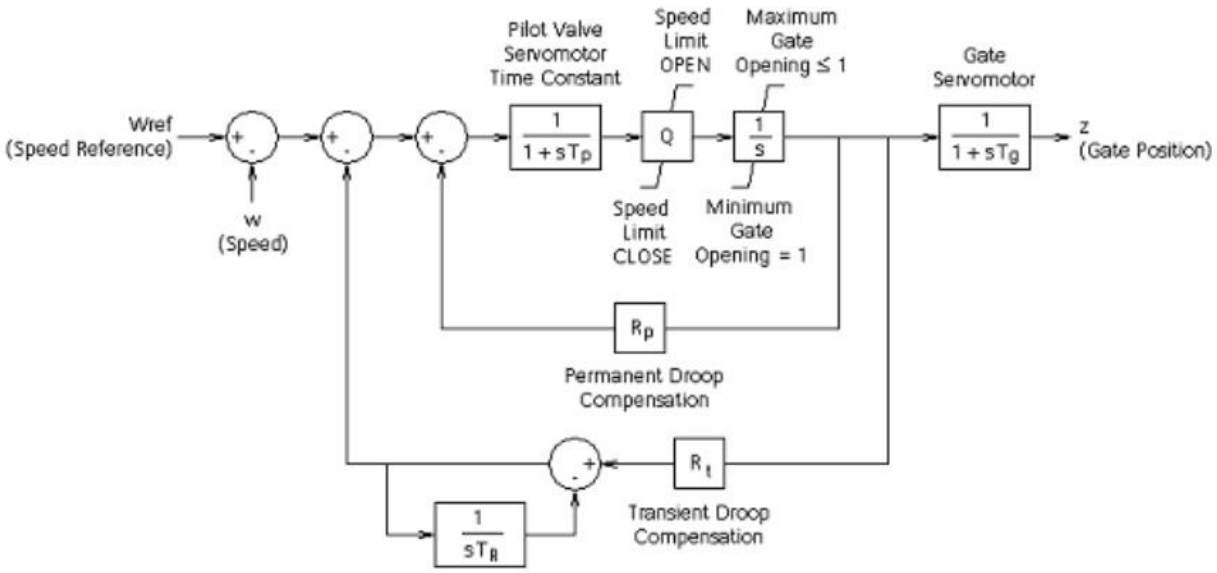

Figure 30: Transfer function of Mechanical-Hydraulic

There are 3 types of IEEE type governor models available in PSCAD.

1.GOV1: Mechanical-Hydraulic Controls
2.GOV2: PID Controls including Pilot and Servo Dynamics
3.GOV3: Enhanced Controls for Load Rejection Studies

GOV1 was selected to be useful for the study and the transfer function of Mechanical-Hydraulic governor in PSCAD is shown in Figure 30 [48]. Q is the servo gain, Rp is the Permeant droop, Rt is the temporary droop, Tg is the mail servo time constant, Tp is the pilot value and servo motor time constant and TR is the reset or dashpot time constant.

5.3 PV Power Plant

5.3.1 Photovoltaic Source

The photovoltaic source is assumed to contain several strings of PV modules connected in parallel, where each string consists of a number of individual PV modules connected in series. All PV modules connected in parallel and series are identical. Temperature and the irradiance have to be given as inputs. Parameters of the PV source are presented in the Appendix C.

5.3.1.1 Modelling of solar cell in PSCAD

PSCAD use the equivalent circuit shows in Figure 31 to model a PV source [49].

$$I = I_G - I_D - I_{SH} \tag{30}$$

I_G is the current generated by the photovoltaic cell. Characteristics of I_G is shown in equation (31). According to equation (31) I_G depends on the cell temperature T_C and the irradiance G on the solar panel. In equation (31), I_{SCR} is the short circuit current at the reference solar irradiation G_R and the reference cell temperature T_{CR}. α_T is the temperature coefficient of photo current.

$$I_G = I_{SCR}\frac{G}{G_R}[1 + \alpha_T(T_C - T_{CR})] \tag{31}$$

Diode current I_D and shunt brunch current I_{SH} in equation (30) is replaced from the equation (32).

$$I = I_G - I_0\left[\exp\left(\frac{V + R_{SR}}{nkT_c/q}\right) - 1\right] - \left(\frac{V + R_{SR}}{R_{SH}}\right) \tag{32}$$

Current I_0 in equation (32) is the dark (saturation current) current. It is a function of the cell temperature as given in equation (33). I_{0R} is the dark current at the reference temperature, q is the charge of an electron and k is the Boltzmann constant. The band-gap energy of the solar cell material is e_g and n represents the diode ideality factor which can take a value in between 1-2.

$$I_0 = I_{0R}\left(\frac{T_C^3}{T_{CR}^3}\right)\exp\left[\frac{1}{T_{CR}} - \frac{1}{T_C}\right]\frac{qe_g}{nk} \tag{33}$$

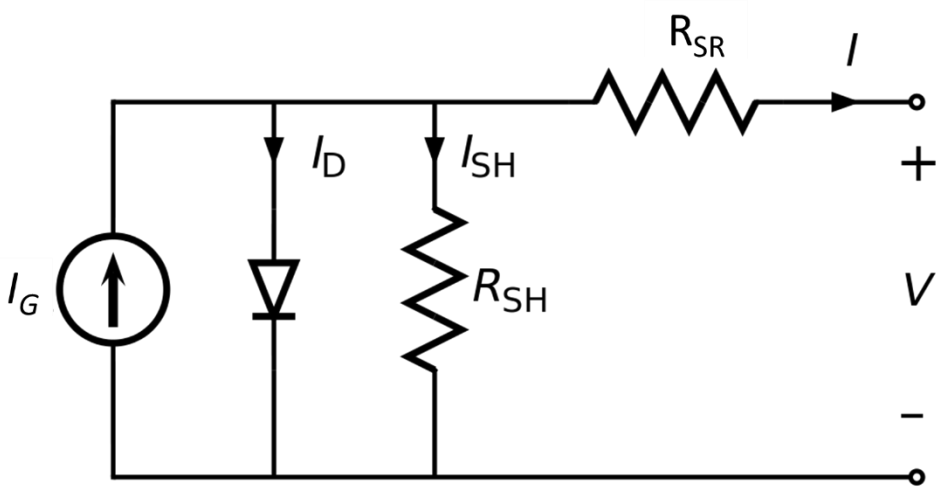

Figure 34: Equivalent circuit of a solar cell used in PSCAD

5.3.2 MPPT Controller

Perturb and Observe algorithm is used as the MPPT algorithm in this study. Parameters of MPPT controller presented in Appendix C.

5.3.3 DC-DC Boost Converter

Figure 32 shows the boost converter used in the simulation. Input side is consists of a low pass filter. Figure 33 shows the gate signal controller to the boost controller. Controller compare the Pref which is generated from the MPPT controller and the dc link power Pdc which is the output power of the boost converter. PI controller will generate the duty cycle to the boost converter, driving the error to zero. P_Lim limits the maximum allowable reference power protecting the boost converter from high currents.

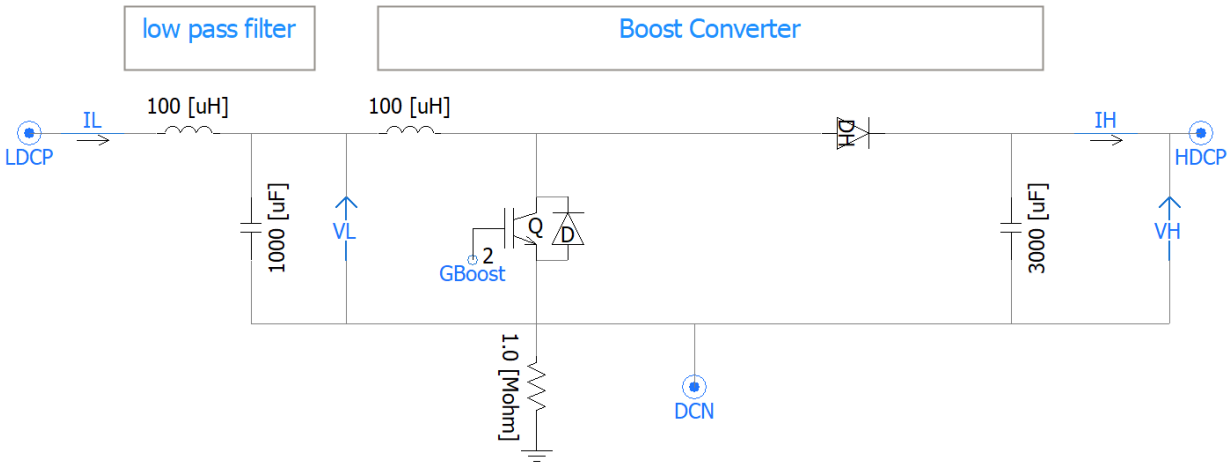

Figure 37: Boost Converter

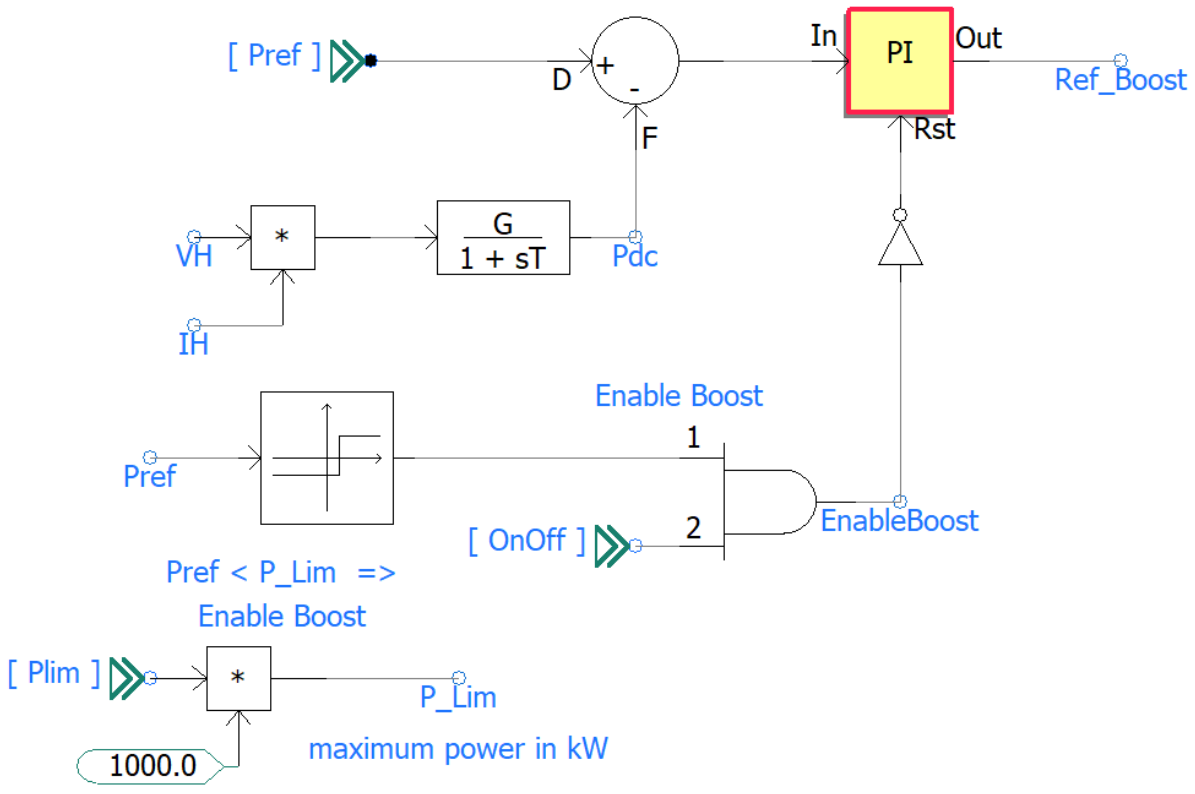

Figure 36: Gate Signal Controller

5.3.4 Voltage Source Converter (VSC)

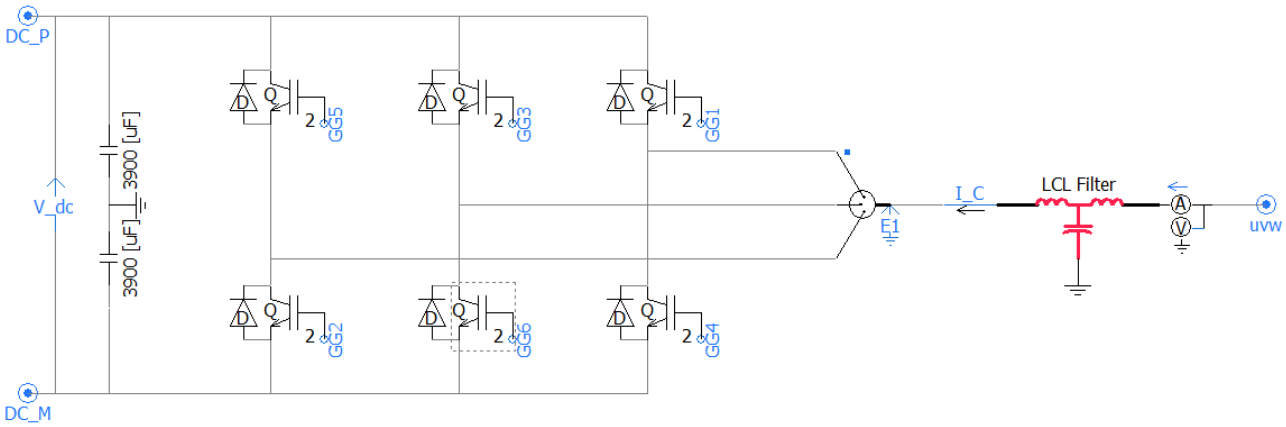

Figure 38: VSC Controller circuit

VSC consist of an inverter circuit with 6 IGBTs as shown in Figure 34. Gate signals are produced by the following controllers:

1. Vdc Controller
2. Id Controller
3. Q Controller
4. Iq Controller

Vdc controller shown in Figure 35(a) is used to produce d axis reference current (idref) by taking the error between the desired voltage across the dc link and the actual voltage of the dc link. This error signal regulated from a PI controller to generate the reference d axis current. This d axis current is generated in a way that dc link voltage is maintained on a desired value. idref is compared with the grid d component current to produce inverter d axis reference voltage(vd1) as shown in Figure 35(b). Id is the component which is corresponding to active power controlling. When a frequency disturbance

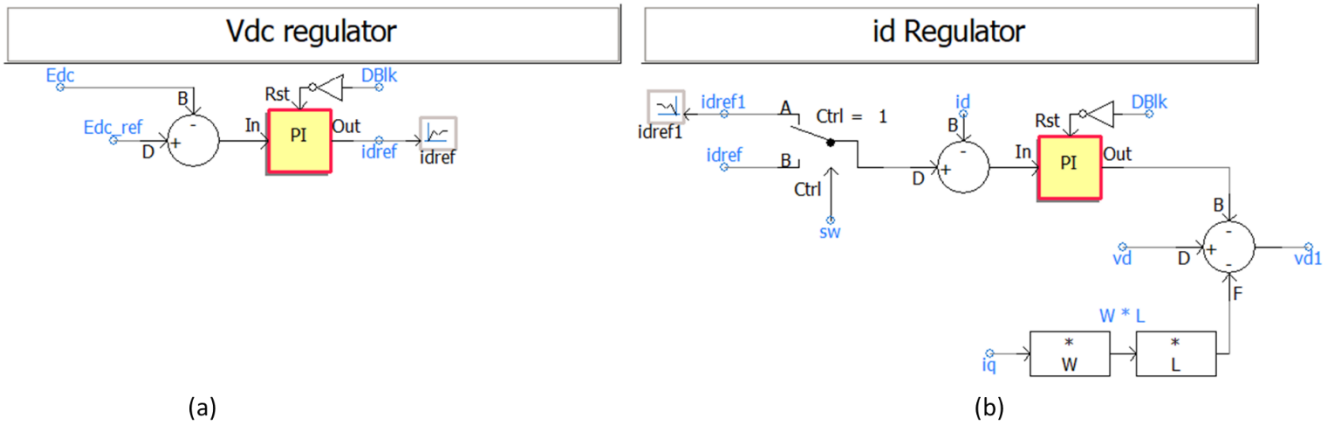

(a) (b)

Figure 35: (a) Vdc Regulator and (b) id regulator

occurs due to a supply demand mismatch, VSM controller will produce a d axis current component (idref1) which is also fed to id controller in Figure 35(b) 'sw' commands switching from normal mode to VSM mode.

Reactive power controlling is regulated from the reactive power reference (Qref). Qref is compared with actual generated reactive power (Q) and the error is fed to a PI controller to generate q axis reference current(iqref) as shown in Figure 36(a). Iq

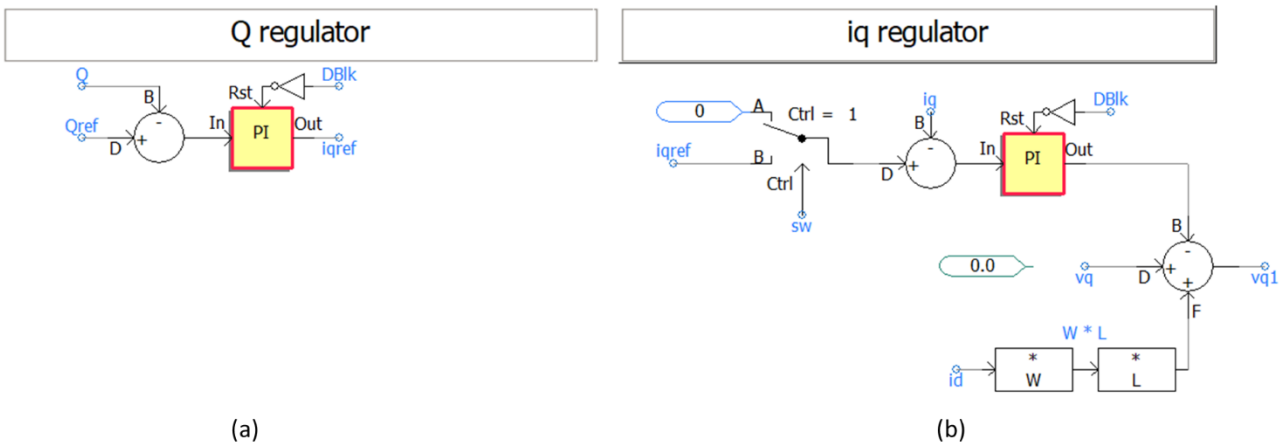

Figure 36: (a) Q regulator and (b) iq regulator

regulator is used to produce the inverter q axis voltage reference(vq1) from the iqref which is generated from Q regulator as shown in Figure 36(b). In this study only active power control is only taken into consideration. Therefore, when VSM algorithm is activated, iqref is driven to zero by 'sw'.

5.3.5 PWM Generator

As shown in Figure 37 d-q axis reference voltages (Vd1 and Vq1) from id regulator and iq regulator are converted into polar format of which. The magnitude is divided by the half the dc link voltage. This value is commonly known as the modulation index. The new amplitude and the angle are converted to rectangular form which are fed to a DQ to ABC converter which uses the continuous phase angle captured by the PLL. Outputs from DQ to ABC transformation are 3-phase inverter reference signals (Ref_a, Ref_b, Ref_c) which are compared against a carrier wave to generated PWM signal to each IGBT in the inverter. PWM generator modelled in PSCAD is presented in Appendix D.

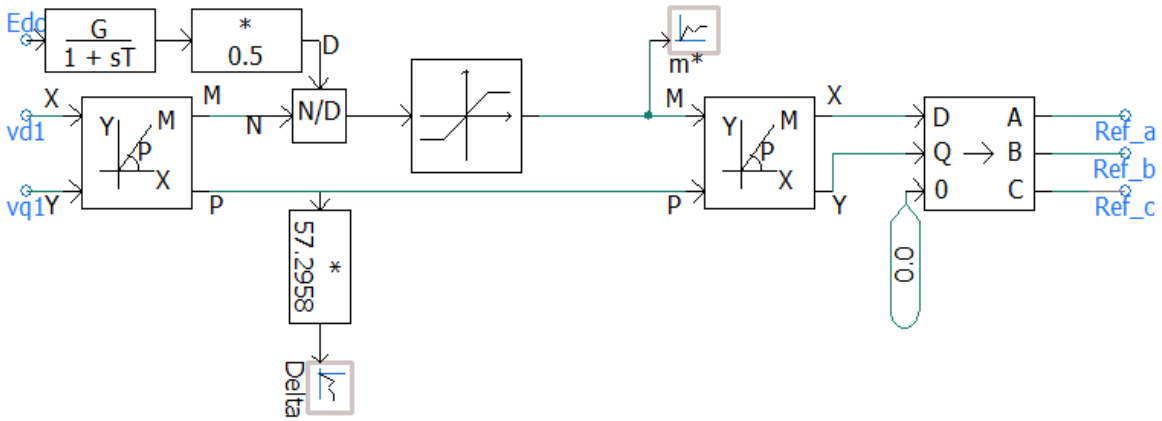

Figure 37: PWM reference wave form generator

5.3.6 Phase Locked Loop (PLL)

A phase-locked loop (PLL) is a control system that generates an output signal whose magnitude is related to the phase of its input signal. PLL tracks the phase angle of a signal continuously. Phase angle from the PLL used to decouple abc components to d-q components and vice versa. It is critical to have an accurately track the phase angle.

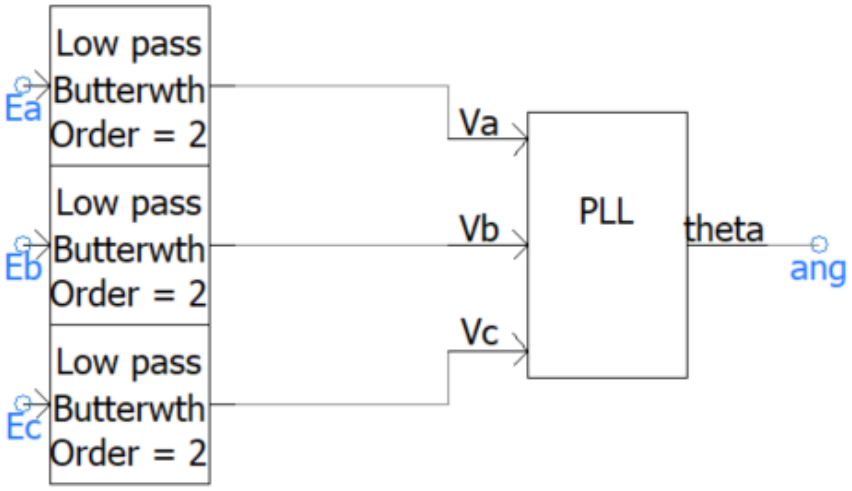

Figure 38: Low pass filter with PLL

However, inverter operation adds harmonics to the system which makes it difficult to track the actual phase angle. Therefore, voltage signals are sent through a low pass filter to remove high frequency components added by inverter switching and to obtain the fundamental component of the voltage signal which is to be fed to the PLL as shown in Figure 38.

5.4 VSM Controller

The simulation model of the VSM controller is shown in Figure 39. Rate limiters and hard limiters are used to keep the controller within margins to avoid any numerical instability conditions which can occur. Furthermore, these limiters reduce the unwanted peaks and oscillations introduced by the VSM.

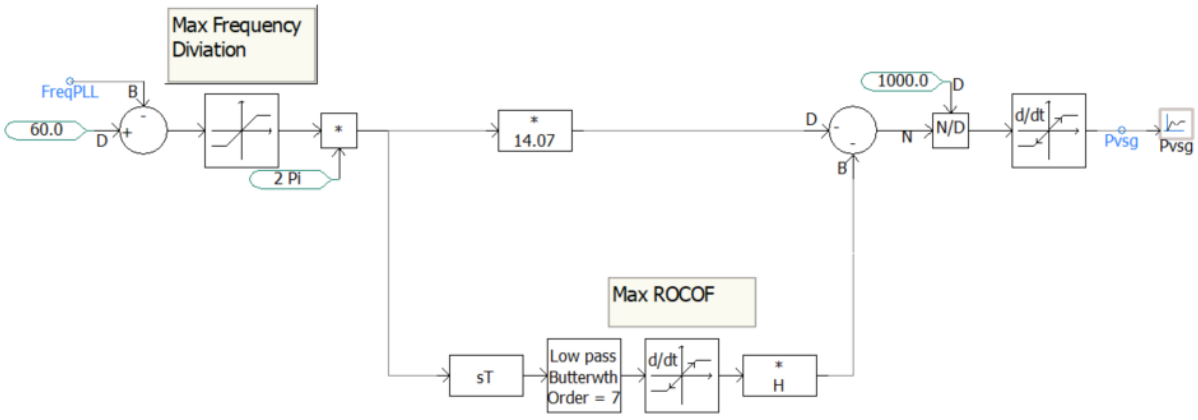

Figure 39: Simulated VSM Controller

5.4.1 Variable Inertia Controller

Variable inertia controller is simulated as shown in Figure 40. Frequency deviation (Freq_Dev) and ROCOF deviation (ROCOF_Dev) is used to identify the operating section in the load angle curve. A comparator identifies the polarity of the frequency deviation and ROCOF. Depending on the region, inertia constant is generated. Generally, the direction is taken by considering whether the value is greater than zero or less than zero.

But in this case rather than taking zero as the reference, there is a dead band introduced with the purpose to ensure that the controller to not to activate until the dead band is passed. This will avoid unnecessary oscillations.

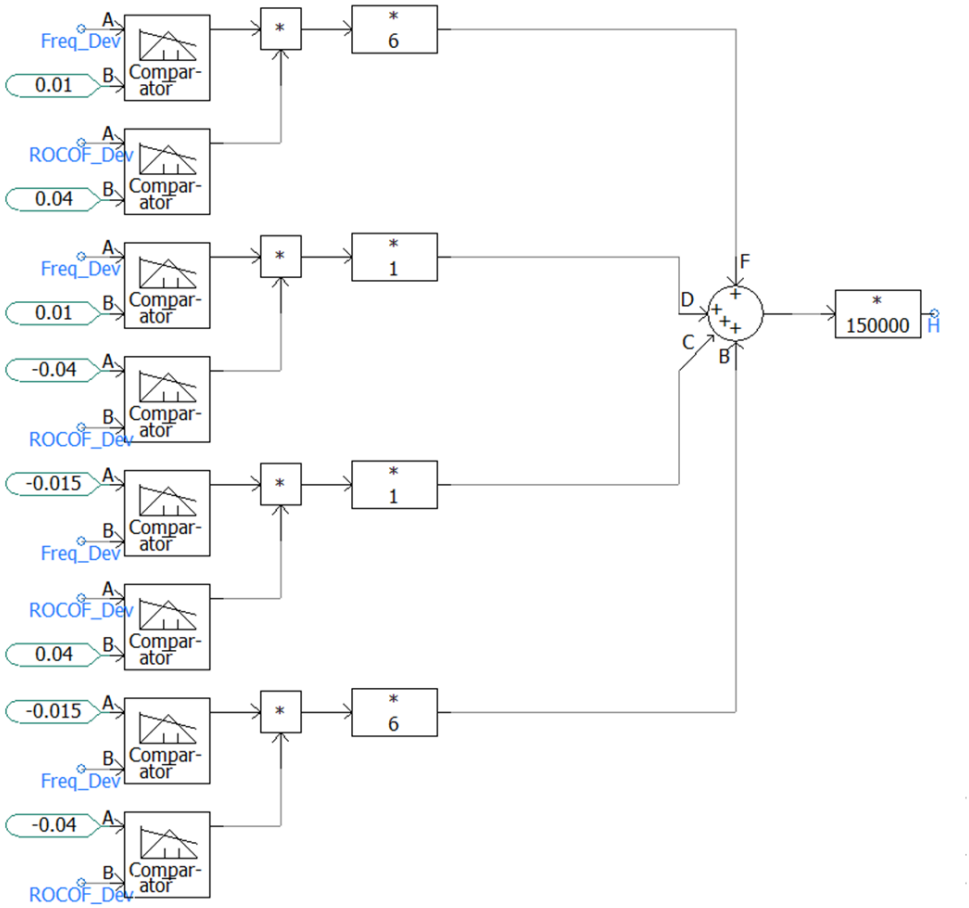

Figure 40: Variable Inertia controller

5.4.2 Current Controller

Current Controller model simulated is shown in Figure 41. Current generated by the PV (idref) is added. A rate limiter is used to avoid sudden inrush current which are higher than component capabilities. This will ensure the safety and the durability of components.

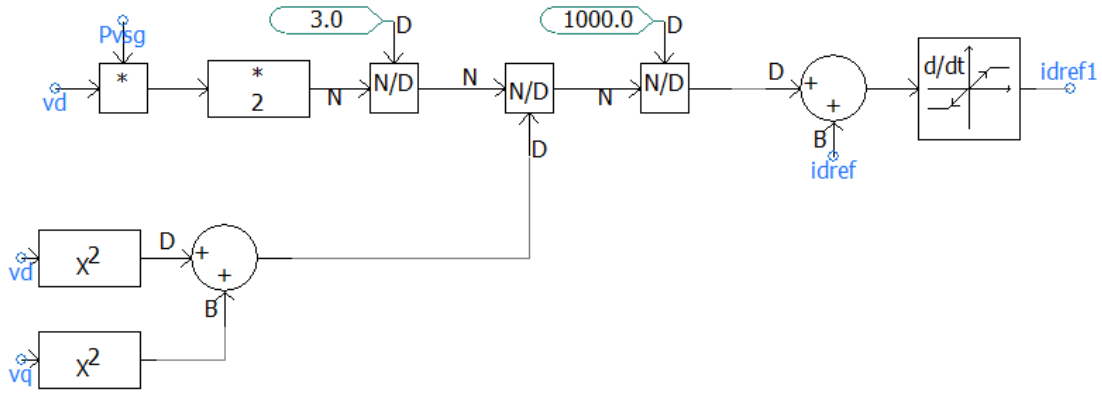

Figure 41: Current Controller

5.4.3 Battery Controller

Buck/Boost converter is used for the battery controller as shown in Figure 42. Controlling of the Buck/Boost converter is done in two layers.

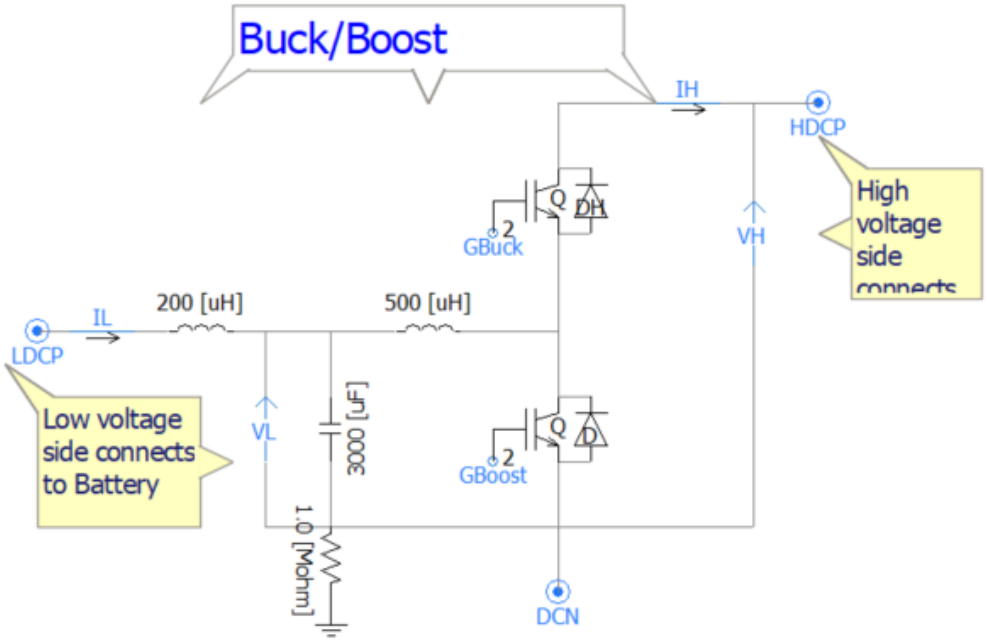

Figure 41: Buck/Boost converter

5.4.4 Upper Level Control

Upper level control, which is shown in Figure 43, is used to define the status of the battery; whether ON or OFF.

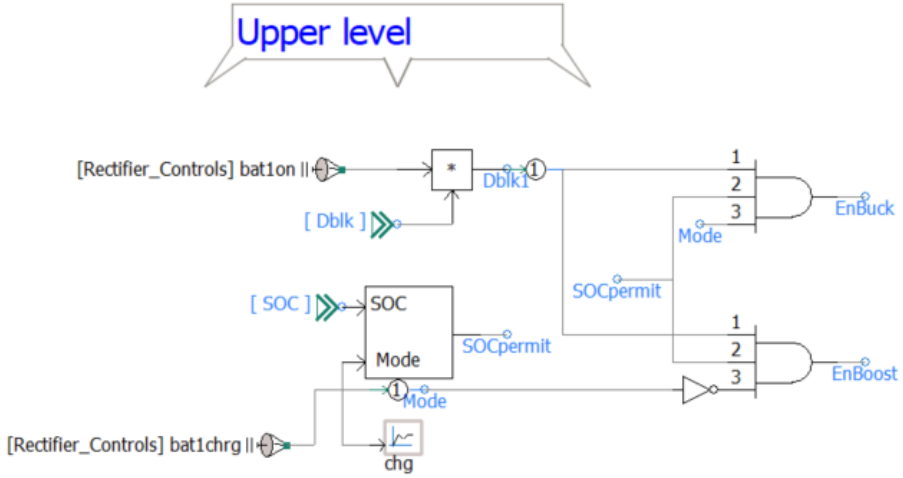

Figure 42: Upper Level Controller

5.4.5 Lower Level Control

Lower level control consists of a boost converter and a buck converter. Boost mode is turned on to discharge batteries as shown in Figure 50. Control signals are provided by EMS. Simulated low level controller is given in appendix E.

5.4.6 PSCAD Battery Model

There are many types of batteries and moreover, many factors affect the performance of a battery. Many mathematical models are available to predict the performance of an actual battery. PSCAD battery model has modelled the behaviour of an electrochemical (rechargeable batteries) based on the[50]. This approach models the battery as an ideal control voltage source with a series resistance as shown in Figure 44.

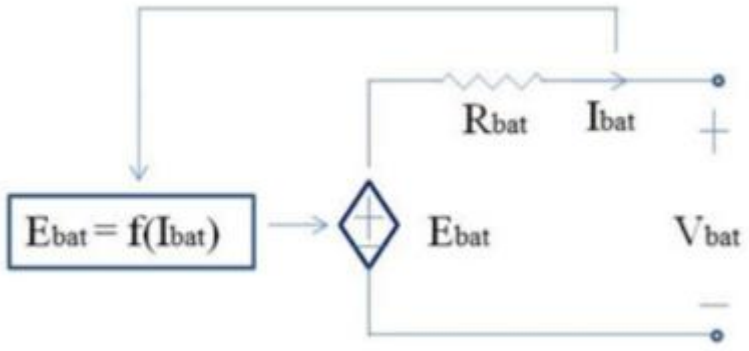

Figure 44: PSCAD battery equivalent circuit

.

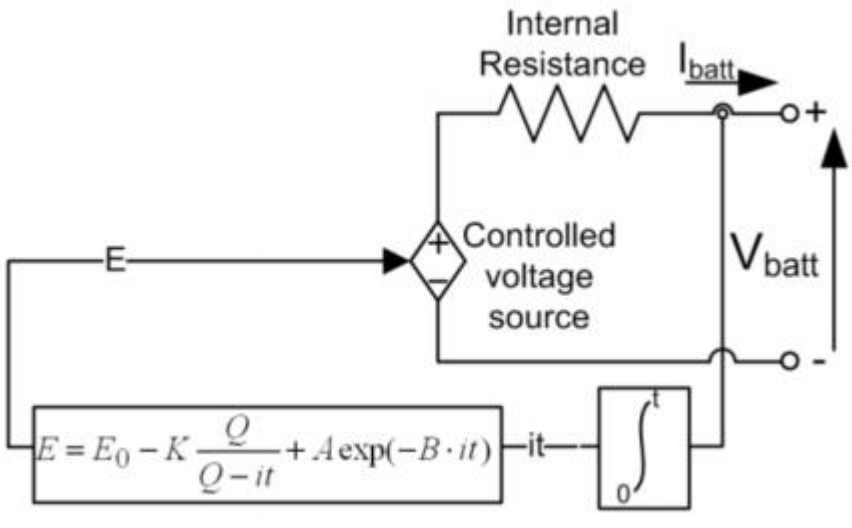

Figure 45: Non linear battery model

In each control cycle source voltage is calculated based on the SOC of the battery by solving non-linear equation given in Figure 53. E is the no-load voltage(V), E0 is battery constant voltage(V), k is the polarization voltage (V), Q is the battery capacity (Ah) $\int i\, dt$ is the actual battery charge (Ah), i is the battery current and B is the inverse of

exponential zone time constant(Ah)-1. This model is based on several assumptions and limitations as listed below.

5.4.6.1 Assumptions

1. Internal resistance is assumed to be constant during the charging and discharging cycles and doesn't vary with the amplitude of the current.
2. Model parameters are deduced from discharge characteristics and assumed to be the same for charging.
3. Capacity of the battery doesn't change with the amplitude of the current (No Peukert effect).
4. The temperature doesn't affect the model's behaviour.
5. Self-Discharge of the battery is not represented.
6. Battery has no memory effect.

5.4.6.2 Limitations

1. Minimum No-Load battery voltage is 0 V and the maximum battery voltage is not limited.
2. Minimum capacity of the battery is 0 Ah and the maximum capacity is not limited. Therefore, the maximum SOC can be greater than 100% if the battery is overcharged.

This model can accurately represent the behaviour of many types of batteries. Model has been validated by comparing the discharging curves with manufacture curves[50]. Figure 46,47,48 shows the comparison of battery model curves with manufacture curves given in datasheets respectively.

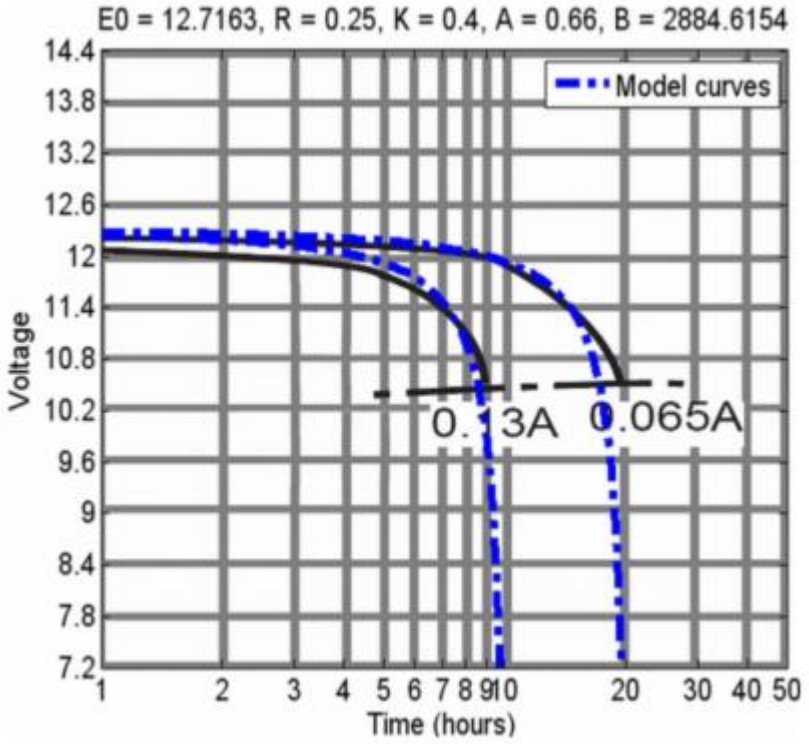

Figure 46: Lead-Acid battery 12V 1.2Ah

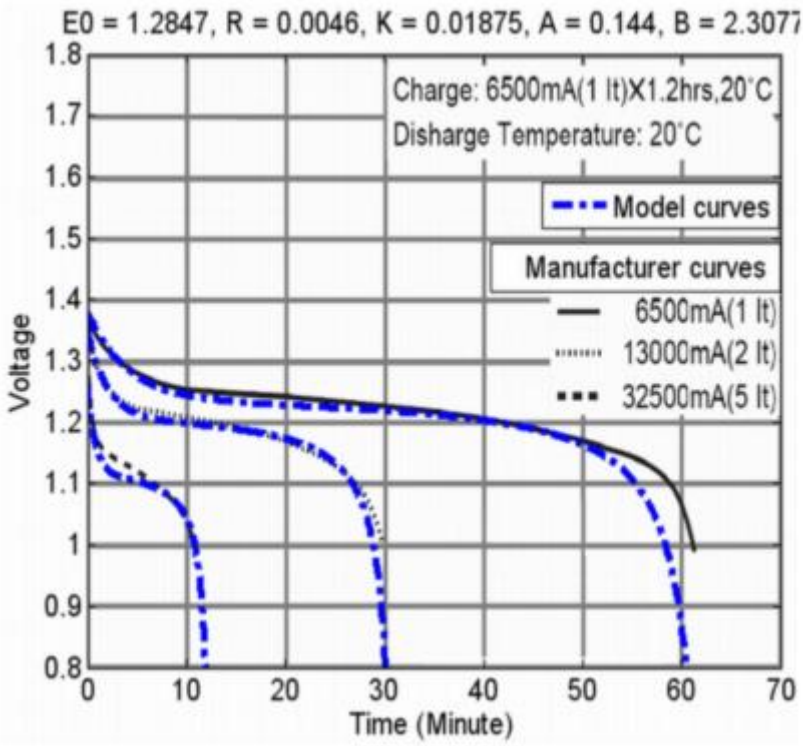

Figure 48: Nickel-Metal-Hydrid battery 1.2V 6.5Ah

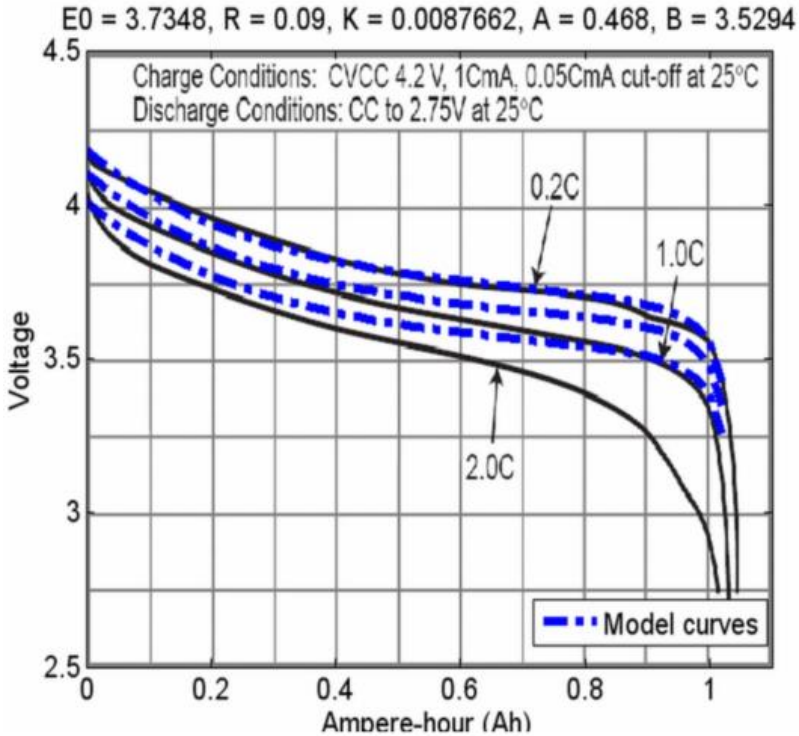

Figure 47: Lithium-Ion battery 3.6V 1Ah

5.5 Energy Management System.

As described in the section 4.4, input data for the energy management system are frequency, calculated power from the VSG algorithm and the power generated by the solar PV. Energy management controller produce 8 outputs which are, battery on/off status for each battery, charge/discharge status for each battery and charging/ discharging power reference for each battery. Figure 49 shows the energy management controller.

Equation 27,28,29,30 has been modelled inside the battery management controller to calculate the reference power. The Energy Management Controller is presented in appendix F.

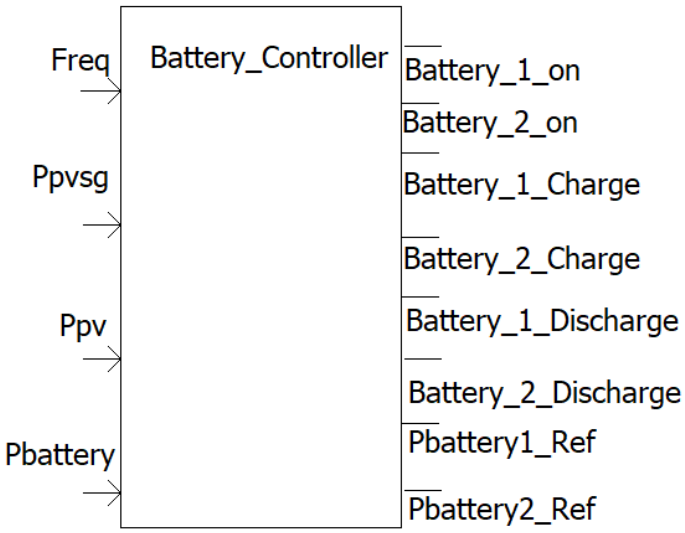

Figure 49: Energy management controller

5.6 Simulated Cases

5.6.1 Case1: Load Adding

This case represents load connection which is equivalent to a sudden loss in generation. Renewable sources such as solar and wind are intermittent and depends on the weather condition and thus the output can suddenly change. From generation point of view, a drop in generation is similar to a sudden addition of a load to the remaining generators.

Initially, breaker is in open state so that the total demand is equal to the fixed load (23 MW). Once the system has reached its steady state, second load (3 MW) is connected by closing the breaker. Transient response is observed with and without the proposed VSM controller and the EMS.

5.6.2 Case 2: Load Disconnecting

This case represents load disconnection which is equivalent to a sudden increase of generation. As described in section 5.6.1, renewable sources highly depends on the weather condition. When there is a sudden increase in wind or solar irradiance (when there is a cloudy situation solar irradiance will drop but when the cloud moves irradiance will suddenly increase), output power will suddenly increase. From the point of generation, this is seen as a sudden load disconnection.

Initially breaker is in close position with both loads connected. Once the system has reached its steady state, breaker is opened and one of the loads will be disconnected suddenly. Transient response is observed with and without the proposed VSM and EMS controllers.

Chapter 6: **Results**

6.1 Case 1

As discussed in the chapter 5, 3MW load is connected at 55s. Frequency is observed without the VSM controller. Frequency has dropped to 57.21 Hz in the first cycle without the VSM and EMS controllers as shown in Figure 50.

The same procedure is repeated with VSM and EMS controllers. Frequency drop is reduced to 58.08Hz in the first cycle as shown in Figure 51. Comparison of these cases are shown in Figure 52. As shown in Figure 52, transient response is enhanced from the VSM and EMS. It decreases the sudden frequency and as a result whole transient response under the disturbance will be reduced, improving the frequency recovery.

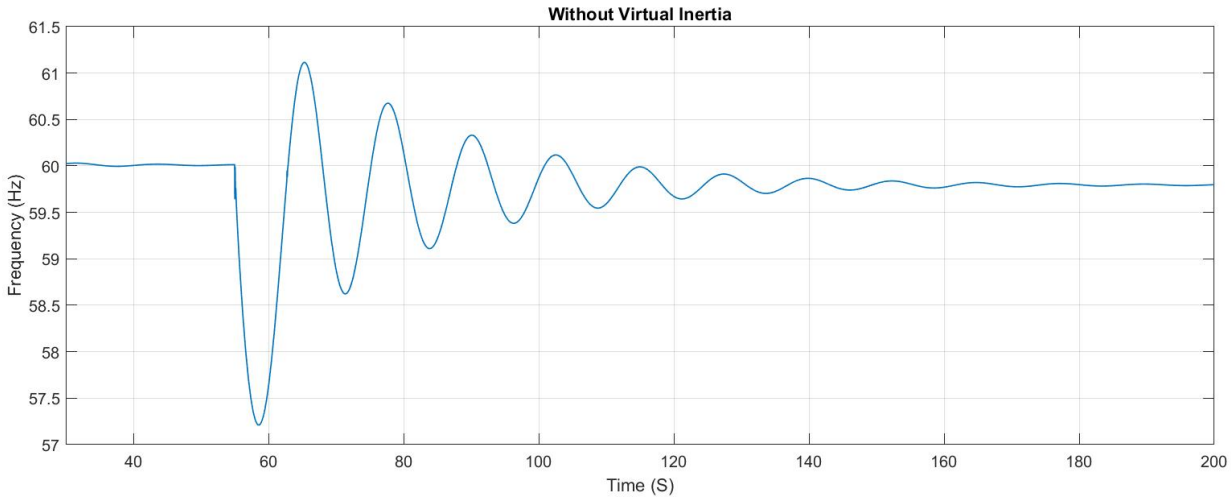

Figure 50 : Load connected situvation without VSM and EMS

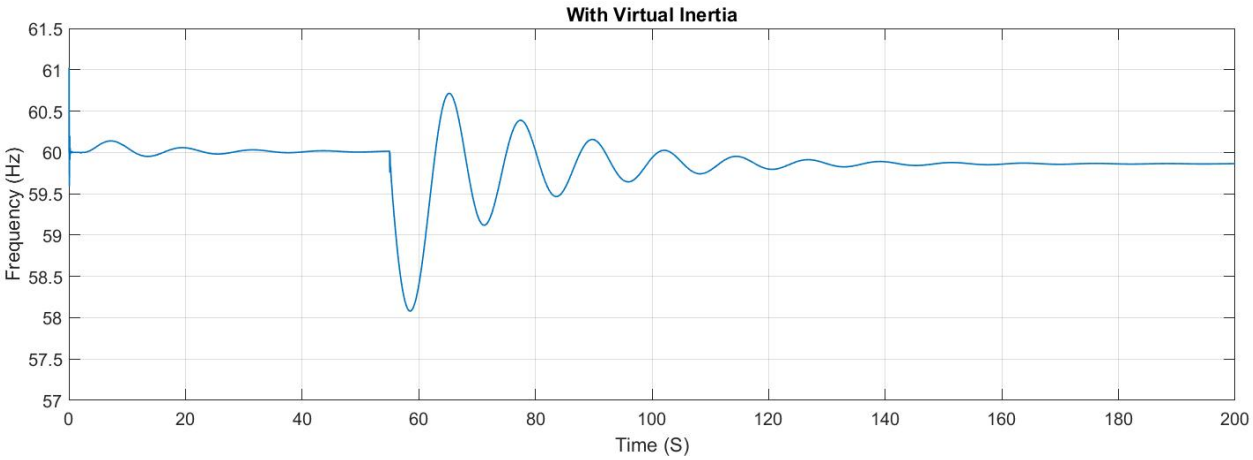

Figure 51: Load connected situvation with VSM and EMS

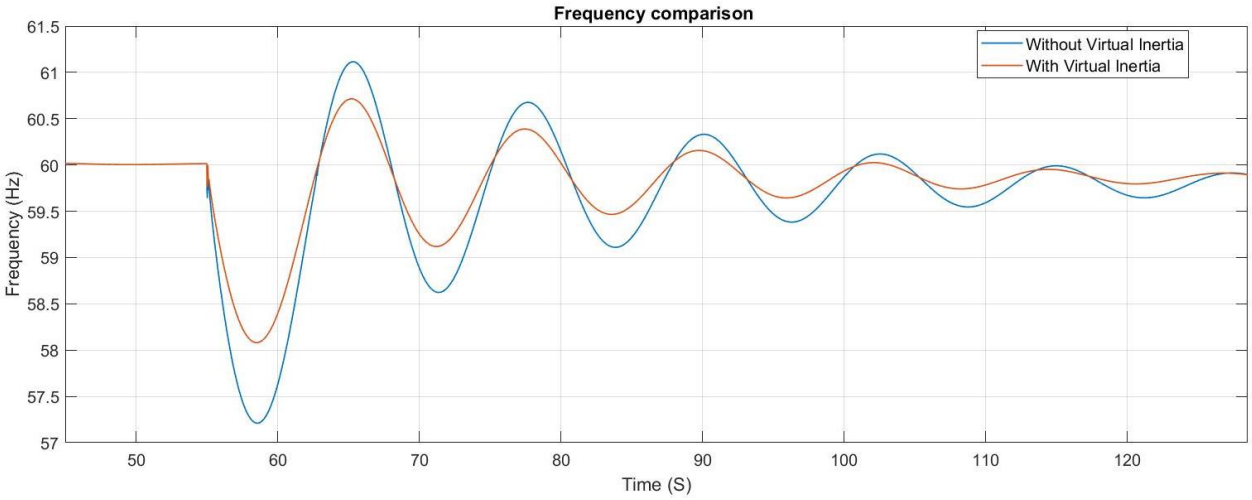

Figure 52: Frequency comparison with and without VSM and EMS

6.2 Case 2

In this case 3MW load is disconnected at 55 s. As shown in Figure 53 frequency is increased up to 63.01Hz immediately following the disconnection. The same procedure was repeated with VSM and EMS and the frequency recovery is shown in Figure 54. It can be seen that the frequency increment in the first cycle has been reduced to 62.02Hz.

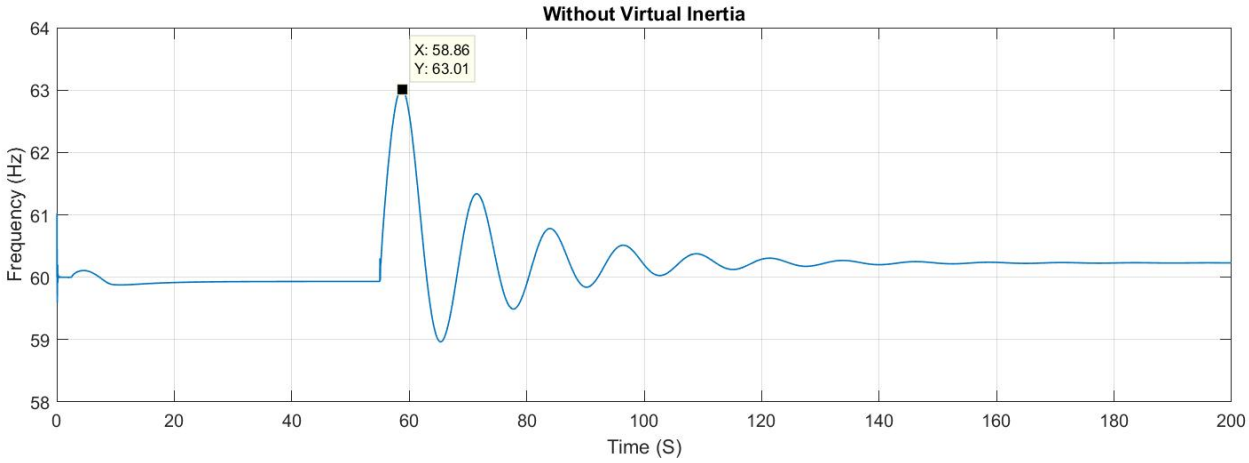

Figure 53: Load disconnected situvation without VSM and EMS

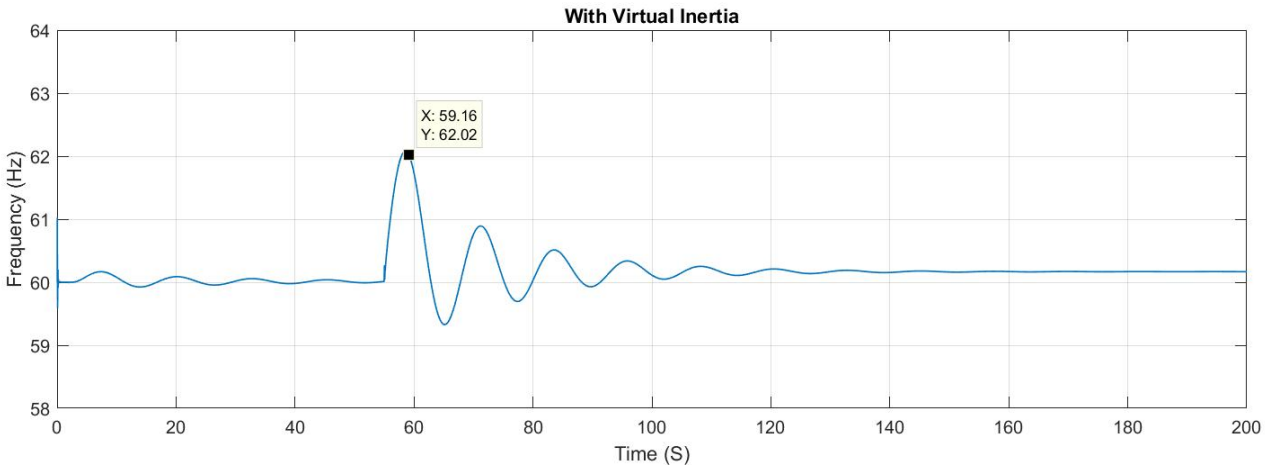

Figure 54 : Load disconnected situvation with VSM and EMS

Figure 55 shows a comparison of both cases. As shown in Figure 55 due to the effect of the VSM and EMS frequency recovery has become much smoother and thus the transient response has been improved.

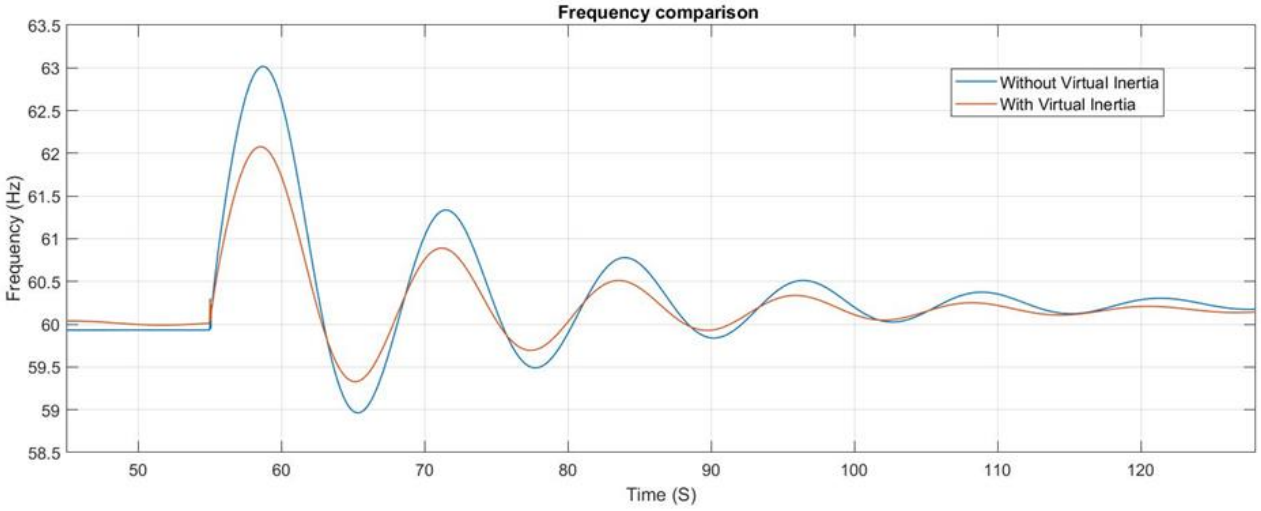

Figure 55 :Frequency comperison with and without VSM and EMS

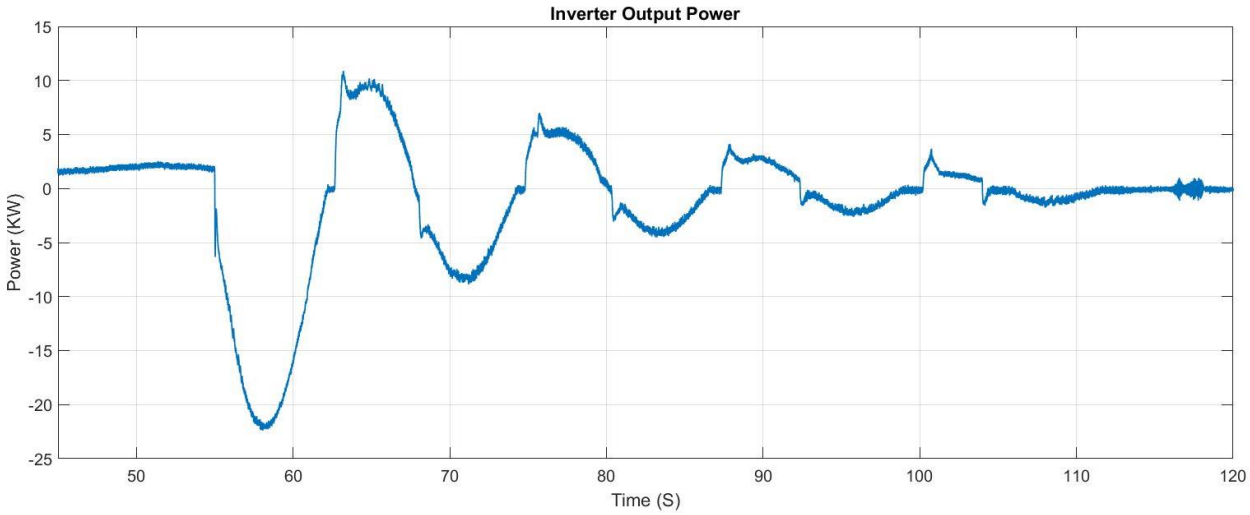

Figure 56 : Inverter output power

Output power of the inverter with VSM and EMS controllers during a load disconnection scenario is shown in Figure 56.

Reference power generated by the VSG algorithm is shown in Figure 57 and the corresponding id current generated is shown in Figure 58. Output of the variable inertia controller is shown in Figure 59. Figure 60 shows the output power of a single battery unit. It is evident from Figure 61, that the PV can operate at its maximum power point and continually produce power without any interruption, even during frequency fluctuations due to the action of the newly proposed controller.

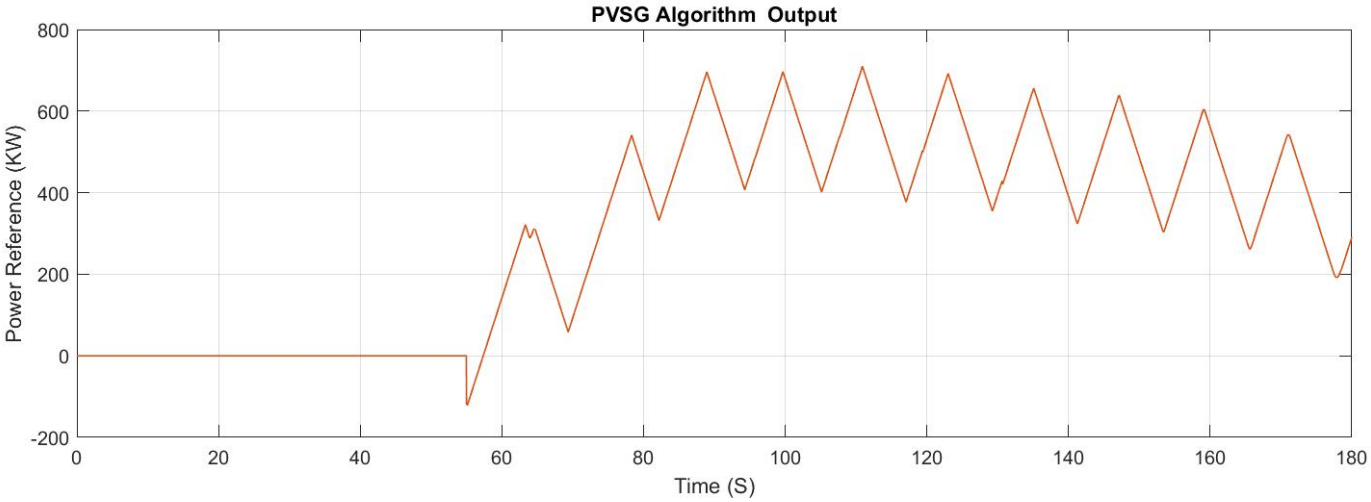

Figure 57: VSG Power reference

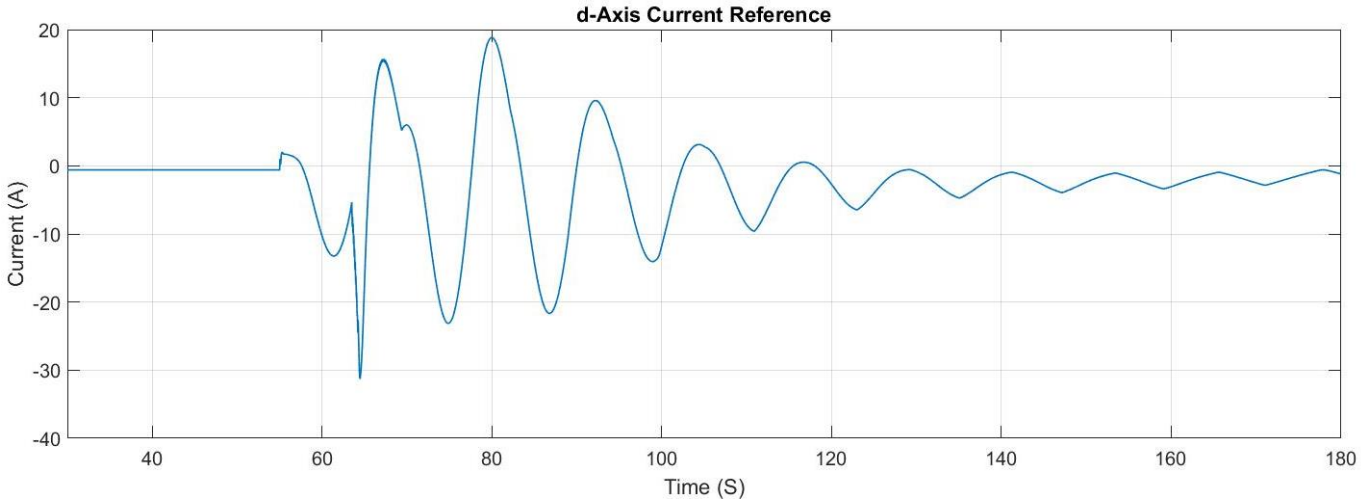

Figure 58: d-axis current reference

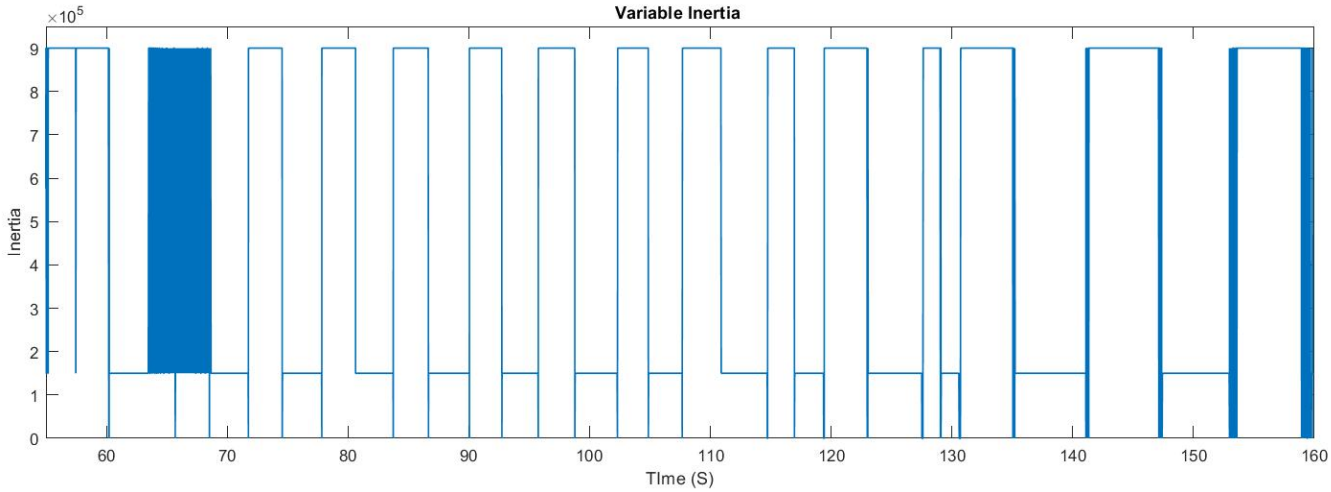

Figure 59: Variable inertia controller output

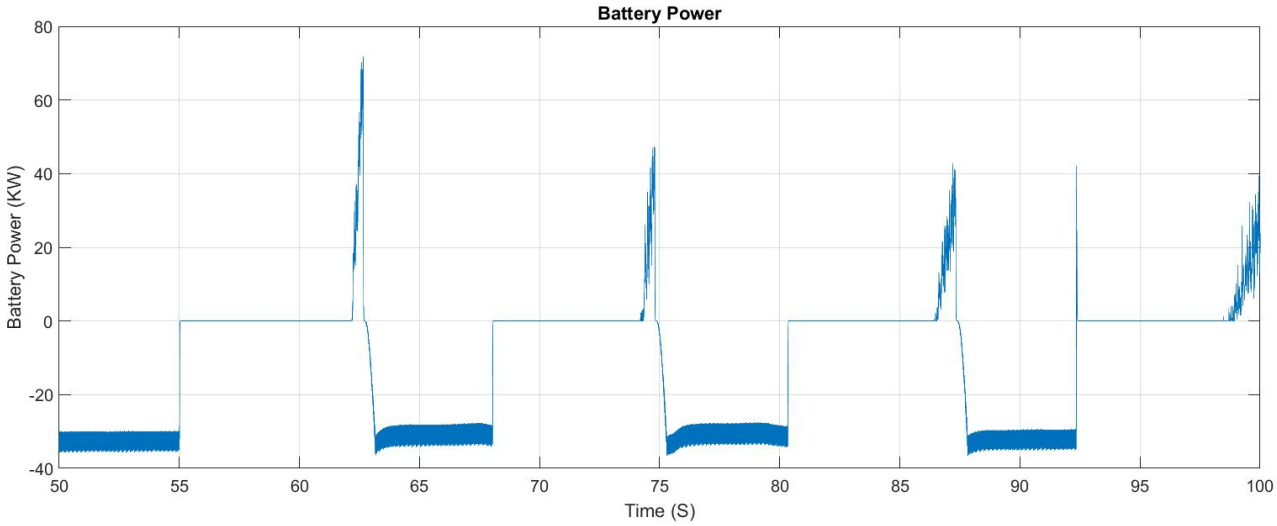

Figure 60 : Output power of battery unit

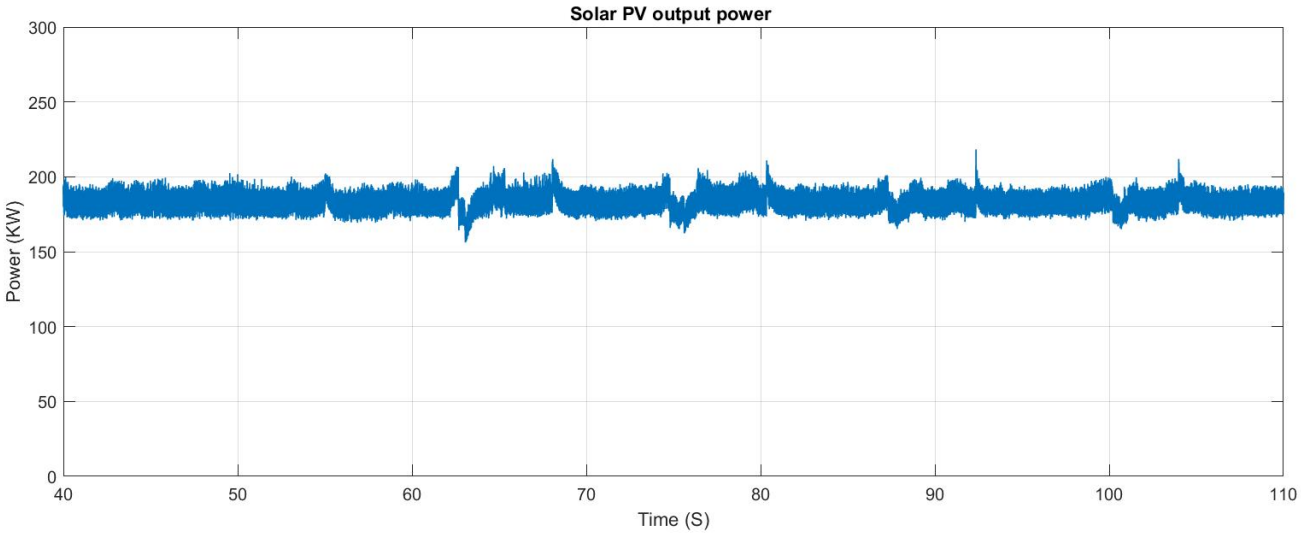

Figure 61: PV output power

Chapter 7: **Discussion**

As seen from results in Chapter 6, VSM and ESM algorithms have enhanced the transient response of the system under sudden disturbances by improving the frequency recovery. This means that the system inertia response has been improved by the proposed VSM controller. Therefore, stress on the primary control has been reduced by the proposed VSM and EMS controllers. Thus, system has recovered faster than that without the controller.

Energy management controller makes it possible to run the solar power plant at its maximum power point even during disturbances and the battery management system always give priority to fulfil the energy requirement within the system through solar PV. Therefore, battery management system reduces the required energy storage capacity.

Lack of inertia in conventional inverter driven power generation sources imposes limits on the capacity of converter-based generation that could be connected to a system. Limits are imposed mainly due to frequency stability issues related with converter-based generation. But with the proposed VSM and energy management controller, inverter driven power plants can emulate the inertia response. Having a variable inertia constant is an added advantage which is not present in traditional generators. Therefore, with the proposed controller inertia response can be given a more dynamic behaviour than like in conventional generators. With these enhanced inertia-support capabilities given by the newly proposed controllers, limitations for adding inverter dominant power plants can be lowered.

Implementation of the proposed controller doesn't require much changes for the existing systems such as primary, secondary, tertiary controls and MPPT control. PV inverters which already consist of energy storages can accommodate the developed controller easily. Conventional power system operation will not be affected from this newly proposed controller. It supports the system operation and increase the transient frequency stability.

Chapter 8: **Conclusion**

Future power gird is inclined more towards eco-friendly renewable power generation. Most of these renewable power generation are inverter dominant. Lack of inertia in inverter dominant power generation degrades the system frequency stability under supply demand mismatches. Therefore, integrating inverter type renewable energy sources are limited by system operators. With the proposed novel controllers, inverter dominant power plants can emulate the inertia response successfully. Furthermore, with the variable inertia controller, inverters can dynamically enhance the inertia response. These controllers can easily be implemented in PV systems which can connect energy storages. Developed controllers will not affect the traditional grid controllers and it can be implemented in any AC Microgrid system. With this novel concept, microgrids are expected to accommodate more inverter type renewable plants with reduced limitations. It will be a great support for the future of eco-friendly power generation. Further research is to be conducted to enhance the reactive power support in order to enhance the voltage stability in inverter dominant power generation. Therefore, much efficient inverters can be produced which has the capability to enhance the both frequency and voltage stability during disturbances.

References

[1] H. J. Smith, “Paris impacts,” *Science (80-.).*, vol. 364, no. 6435, pp. 39.6-40, 2019.

[2] B. Kroposki *et al.*, “Achieving a 100% Renewable Grid: Operating Electric Power Systems with Extremely High Levels of Variable Renewable Energy,” *IEEE Power Energy Mag.*, vol. 15, no. 2, pp. 61–73, 2017.

[3] B. Cleary, A. Duffy, B. Bach, A. Vitina, A. O’Connor, and M. Conlon, “Estimating the electricity prices, generation costs and CO2 emissions of large scale wind energy exports from Ireland to Great Britain,” *Energy Policy*, vol. 91, no. 2016, pp. 38–48, 2016.

[4] ADB and UNDP, “Assessment of Sri Lanka’s Power Sector-100% Electricity Generation Through Renewable Energy by 2050,” p. 122, 2017.

[5] IEA PVPS, *Trends 2016 in Photovoltaic Applications: Survey Report of Selected IEA Countries between 1992 and 2015*. 2016.

[6] “The Sunshot Initiative.,” *Office of ENERGY EFFICIENCY & RENEWABLE ENERGY*. [Online]. Available: https://www.energy.gov/eere/solar/sunshot-initiative. [Accessed: 18-Jan-2020].

[7] M. Ram *et al.*, “GLOBAL ENERCY SYSTEM BASED ON 100% RENEWABLE ENERGY - POWER SECTOR. Study by Lappeenranta University of Technology and Energy Watch Group, Lappeenranta, Berlin, Nowember 2017,” 2017.

[8] F. Blaabjerg, K. Ma, and D. Zhou, “Power electronics and reliability in renewable energy systems,” *IEEE Int. Symp. Ind. Electron.*, pp. 19–30, 2012.

[9] U. Tamrakar, D. Shrestha, M. Maharjan, B. P. Bhattarai, T. M. Hansen, and R. Tonkoski, “Virtual inertia: Current trends and future directions,” *Appl. Sci.*, vol. 7, no. 7, 2017.

[10] J. Eto *et al.*, “Use of Frequency Response Metrics to Assess the Planning and Operating Requirements for Reliable Integration of Variable Renewable Generation,” no. December 2010, p. LBNL-4142E, 2010.

[11] P. Kundur, *Power System Stability and Control*. New York: McGraw-Hill, 1994.

[12] M. Dreidy, H. Mokhlis, and S. Mekhilef, “Inertia response and frequency control

techniques for renewable energy sources: A review," *Renew. Sustain. Energy Rev.*, vol. 69, no. November 2015, pp. 144–155, 2017.

[13] U. Tamrakar, D. Shrestha, M. Maharjan, B. P. Bhattarai, T. M. Hansen, and R. Tonkoski, "Virtual inertia: Current trends and future directions," *Appl. Sci.*, vol. 7, no. 7, pp. 1–29, 2017.

[14] "Electricity Ten Year Statement (ETYS)," 2014. .

[15] "UK Future Energy Scenarios," 2013. [Online]. Available: http://www2.nationalgrid.com/%0AWorkArea/DownloadAsset.aspx?Id=10451. [Accessed: 18-Jan-2020].

[16] H. P. Beck and R. Hesse, "Virtual synchronous machine," *2007 9th Int. Conf. Electr. Power Qual. Util. EPQU*, 2007.

[17] Q. C. Zhong and G. Weiss, "Synchronverters: Inverters that mimic synchronous generators," *IEEE Trans. Ind. Electron.*, vol. 58, no. 4, pp. 1259–1267, 2011.

[18] R. Hesse, D. Turschner, and H. P. Beck, "Micro grid stabilization using the virtual synchronous machine (VISMA)," *Renew. Energy Power Qual. J.*, vol. 1, no. 7, pp. 676–681, 2009.

[19] Y. Chen, R. Hesse, D. Turschner, and H. P. Beck, "Improving the grid power quality using virtual synchronous machines," *Int. Conf. Power Eng. Energy Electr. Drives*, no. May, pp. 1–6, 2011.

[20] Y. Hirase, K. Abe, K. Sugimoto, and Y. Shindo, "A grid-connected inverter with virtual synchronous generator model of algebraic type," *Electr. Eng. Japan (English Transl. Denki Gakkai Ronbunshi)*, vol. 184, no. 4, pp. 10–21, 2013.

[21] K. Sakimoto, Y. Miura, and T. Ise, "Stabilization of a power system with a distributed generator by a Virtual Synchronous Generator function," *8th Int. Conf. Power Electron. - ECCE Asia "Green World with Power Electron. ICPE 2011-ECCE Asia*, no. 2, pp. 1498–1505, 2011.

[22] D. Remon, A. M. Cantarellas, J. D. Nieto, W. Zhang, and P. Rodriguez, "Aggregated model of a distributed PV plant using the synchronous power controller," *IEEE Int. Symp. Ind. Electron.*, vol. 2015-Septe, pp. 654–659, 2015.

[23] J. Alipoor, Y. Miura, and T. Ise, “Power system stabilization using virtual synchronous generator with alternating moment of inertia,” *IEEE J. Emerg. Sel. Top. Power Electron.*, vol. 3, no. 2, pp. 451–458, 2015.

[24] M. P. N. Van Wesenbeeck, S. W. H. De Haan, P. Varela, and K. Visscher, “Grid tied converter with virtual kinetic storage,” *2009 IEEE Bucharest PowerTech Innov. Ideas Towar. Electr. Grid Futur.*, no. 1, pp. 1–7, 2009.

[25] F. Katiraei and M. R. Iravani, “Power management strategies for a microgrid with multiple distributed generation units,” *IEEE Trans. Power Syst.*, vol. 21, no. 4, pp. 1821–1831, 2006.

[26] N. Pogaku, M. Prodanović, and T. C. Green, “Modeling, analysis and testing of autonomous operation of an inverter-based microgrid,” *IEEE Trans. Power Electron.*, vol. 22, no. 2, pp. 613–625, 2007.

[27] N. Ertugrul, “Battery storage technologies, applications and trend in renewable energy,” *IEEE Int. Conf. Sustain. Energy Technol. ICSET*, vol. 0, pp. 420–425, 2017.

[28] H. Budde-Meiwes *et al.*, “A review of current automotive battery technology and future prospects,” *Proc. Inst. Mech. Eng. Part D J. Automob. Eng.*, vol. 227, no. 5, pp. 761–776, 2013.

[29] B. Dunn, H. Kamath, and J. M. Tarascon, “Electrical energy storage for the grid: A battery of choices,” *Science (80-.).*, vol. 334, no. 6058, pp. 928–935, 2011.

[30] “Sunrun’s Brightbox Specifications.” [Online]. Available: https://www.sunrun.com/solar-battery-storage/battery-specs. [Accessed: 18-Jan-2020].

[31] D. T. Ton and M. A. Smith, “The U.S. Department of Energy’s Microgrid Initiative,” *Electr. J.*, vol. 25, no. 8, pp. 84–94, 2012.

[32] C. M. Franck, “HVDC circuit breakers: A review identifying future research needs,” *IEEE Trans. Power Deliv.*, vol. 26, no. 2, pp. 998–1007, 2011.

[33] M. G. Simões *et al.*, “Smart-grid technologies and progress in Europe and the USA,” *IEEE Energy Convers. Congr. Expo. Energy Convers. Innov. a Clean Energy Futur. ECCE 2011, Proc.*, pp. 383–390, 2011.

[34] Z. Shuai *et al.*, “Microgrid stability: Classification and a review,” *Renew. Sustain. Energy Rev.*, vol. 58, pp. 167–179, 2016.

[35] W. Yibo and X. Honghua, “Research and practice of designing hydro/photovoltaic hybrid power system in microgrid,” *Conf. Rec. IEEE Photovolt. Spec. Conf.*, pp. 1509–1514, 2013.

[36] M. A. Elgendy, B. Zahawi, S. Member, and D. J. Atkinson, “Assessment of Perturb and Observe MPPT Algorithm Implementation Techniques for PV Pumping Applications,” vol. 3, no. 1, pp. 21–33, 2012.

[37] H. Malek and Y. Chen, “BICO MPPT : A Faster Maximum Power Point Tracker and Its Application for Photovoltaic Panels,” vol. 2014, no. Ic, 2014.

[38] U. Tamrakar *et al.*, “Comparative analysis of current control techniques to support virtual inertia applications,” *Appl. Sci.*, vol. 8, no. 12, 2018.

[39] K. Visweswara, “An Investigation Of Incremental Conductance Based Maximum Power Point Tracking For Photovoltaic System,” *Energy Procedia*, vol. 54, pp. 11–20, 2014.

[40] S. Z. Mirbagheri, S. Mekhilef, and S. M. Mirhassani, “MPPT with Inc . Cond method using conventional interleaved boost converter,” *Energy Procedia*, vol. 42, pp. 24–32, 2013.

[41] MathWorks, “MPPT Algorithm.” [Online]. Available: https://www.mathworks.com/solutions/power-electronics-control/mppt-algorithm.html. [Accessed: 18-Jan-2020].

[42] V. Karapanos, S. W. . De Haan, and K. Zwetsloot, “Testing a Virtual Synchronous Generator in a Real Time Simulated Power System,” *Int. Conf. Power Syst. Transients IPST 2011*, vol. 31, no. February, 2011.

[43] H. Bevrani, T. Ise, and Y. Miura, “Virtual synchronous generators : A survey and new perspectives,” *Int. J. Electr. POWER ENERGY Syst.*, vol. 54, pp. 244–254, 2014.

[44] L. Malesani and P. Tomasin, “PWM Current Control Techniques of Voltage Source Converters - A Survey,” pp. 670–675.

[45] A. Rizqiawan, P. Hadi, and G. Fujita, “Development of grid-connected inverter

experiment modules for microgrid learning," *Energies*, vol. 12, no. 3, pp. 1–16, 2019.

[46] PES, *IEEE Recommended Practice for Excitation System Models for Power System Stability Studies*, vol. 2005, no. April. 2006.

[47] NEPLAN AG, "Exciter models - Standard Dynamic Excitation Systems in NEPLAN Power System Analysis Tool," pp. 1–185, 2013.

[48] J. Oliver, "[1] J. Oliver, 'HYDRAULIC TURBINE AND TURBINE CONTROL MODELS FOR SYSTEM PYNAMIC STUDIES,' J. Chem. Inf. Model., vol. 53, no. 9, pp. 1689–1699, 2013.HYDRAULIC TURBINE AND TURBINE CONTROL MODELS FOR SYSTEM PYNAMIC STUDIES," *J. Chem. Inf. Model.*, vol. 53, no. 9, pp. 1689–1699, 2013.

[49] A. D. Rajapakse and D. Muthumuni, "Simulation tools for photovoltaic system grid integration studies," *2009 IEEE Electr. Power Energy Conf. EPEC 2009*, pp. 1–5, 2009.

[50] O. Tremblay, L. A. Dessaint, and A. I. Dekkiche, "A generic battery model for the dynamic simulation of hybrid electric vehicles," *VPPC 2007 - Proc. 2007 IEEE Veh. Power Propuls. Conf.*, no. August 2015, pp. 284–289, 2007.

Appendix A: PSCAD Synchronous Generator Parameters

Machine name	HydroGener
No. of Q-axis Damper Windings	One
Data Entry format	Generator
Multimass interface	Disable
Armature resistance as	Resistance
D-axis Saturation	Disable
Type of settings for inertial condition	Nine
Machine scale factor	No
External Neutral Connection	Disable
Rates RMS Line-to-Neutral Voltage	10[kV]
Rated RMS Line Current	1.01[kA]
Base Angular Frequency	60 [Hz]
Inertia Constant	2 [S]
Mechanical Friction and Windage	0.05 [p.u]
Neutral Series Resistance	1.0E4 [p.u]
Neutral Series Reactance	0 [p.u]
Iron Loss Resistance	300 [p.u]

Appendix B: Turbine Parameters

Head at rated conditions	10.[p.u]
Output Power at rated conditions	10.[p.u]
Gate position at rated conditions	10.[p.u]
Rated No-Load conditions	Flow
Rated No-Load Flow	0.05[p.u]
Water Starting Time	20 [sec]
Penstock Head Loss Coefficient	0.02 [p.u]
Turbine Damping Constant	0.5
Elastic water Column	No
Surge Tank	No
Input Signal for jet deflector required	No
Input Signal for relief valve required	No
Turbine Status	InitGv

Appendix C: Solar PV and MPPT Parameters

PV array name	PVarray
Number of modules connected in series per array	22
Number of module strings in parallel per array	250
Number of module strings in parallel per array	36
Number of cells connected in series per module	1
Reference irradiation	1000
Reference cell temperature	25
PV array short circuit current	0.488[kA]
PV array open circuit voltage	0.7[kV]
Sampling Interval	0.01
Initial Value of vmpp	0.64 [kV]
Tracking Algorithm	Pretub & Observe

Appendix D: PWM Signal Generator

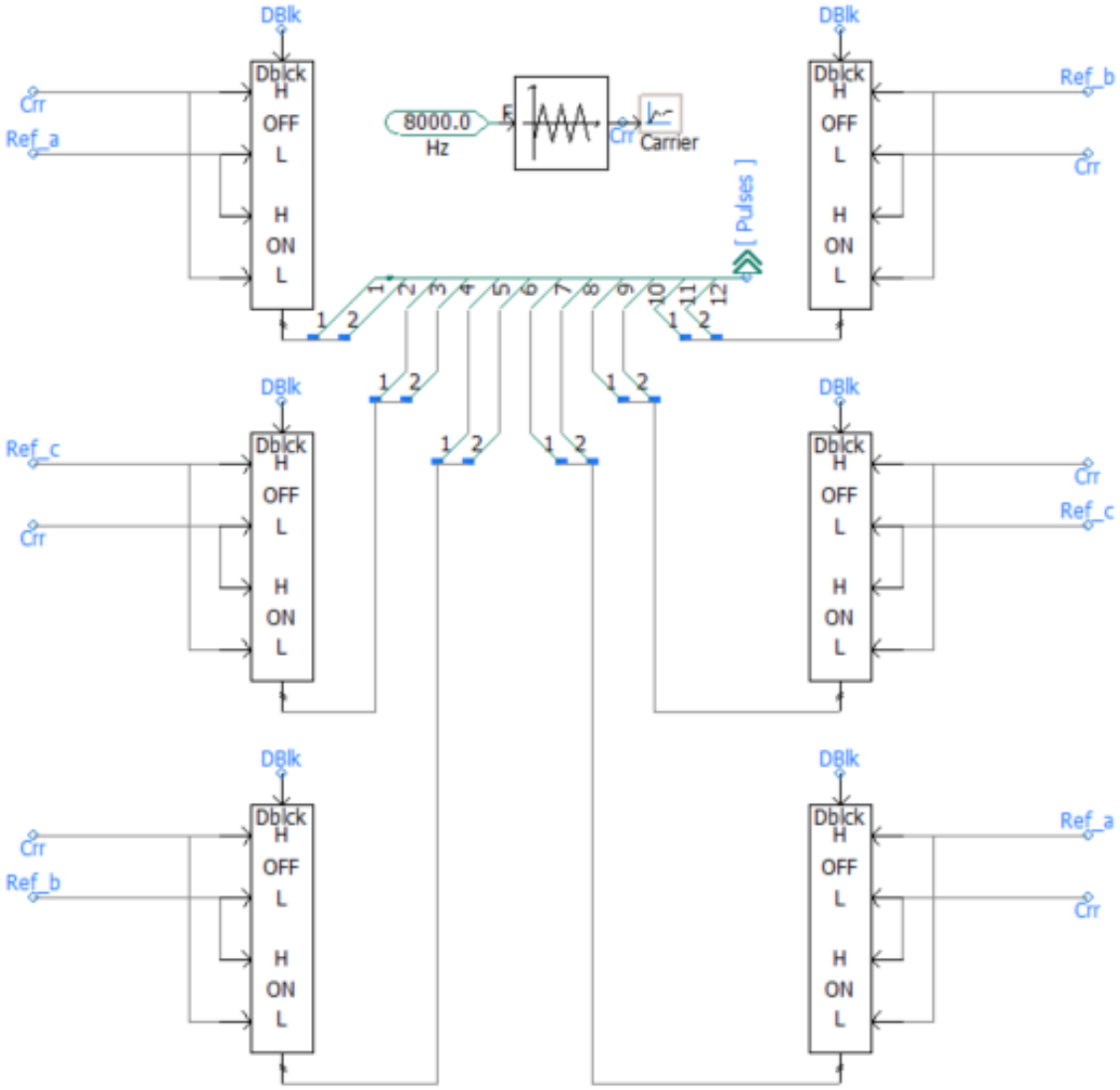

Appendix E: Low level control of the buck boost controller

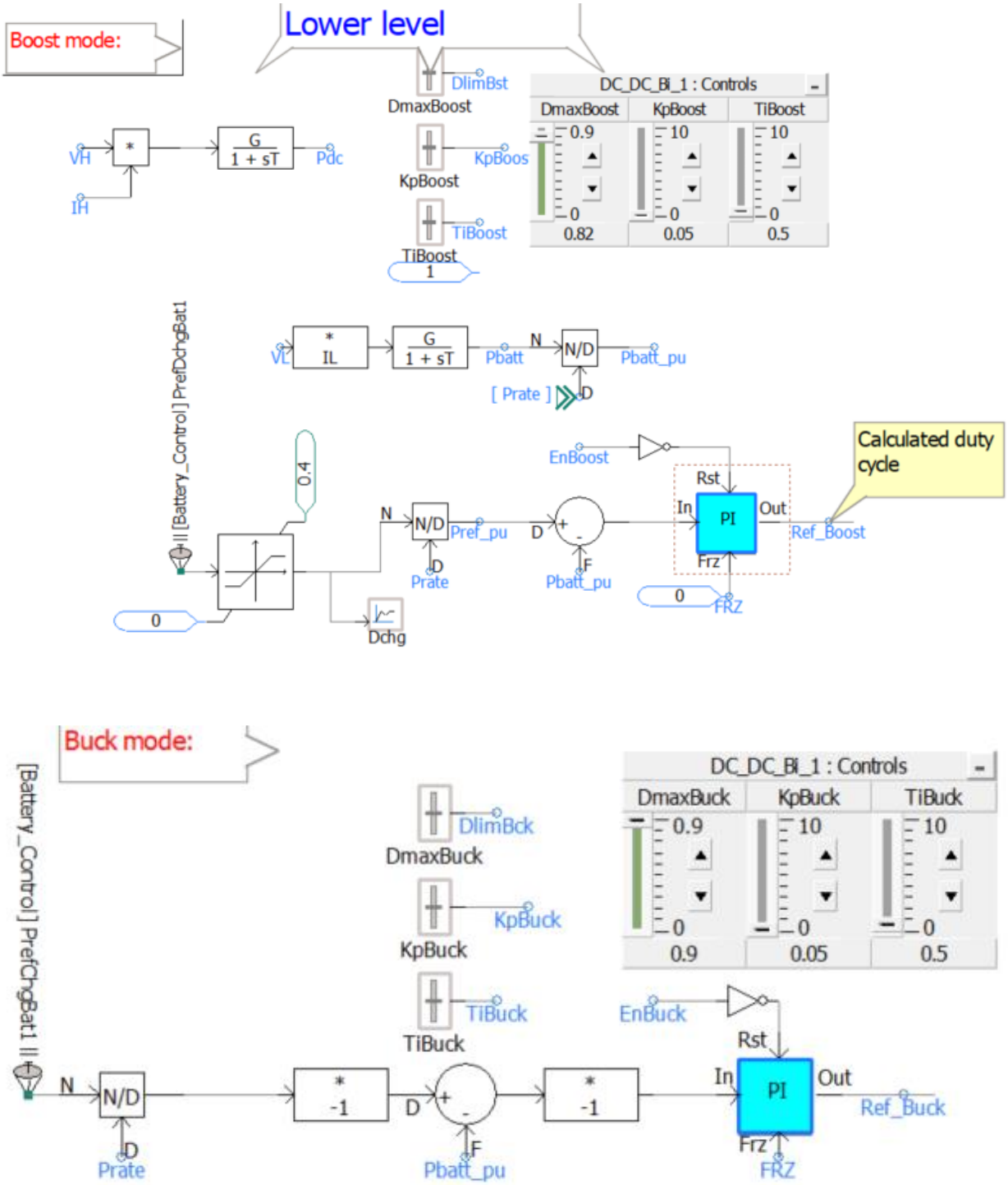

Appendix F: Battery Reference Power Controller